Nanoscale

REVIEW

View Article Online
View Journal | View Issue

Cite this: *Nanoscale*, 2025, **17**, 20670

Strategies for fabricating aligned nano- and microfiber scaffolds: an overview for cell culture applications

Kristina Peranidze, [a,b] Nataraja Sekhar Yadavalli, [b,c] Brianna Blevins,[b] Mikhail Parker,[a,b] Tushita Jain,[a] Mohammad Aghajohari, [a,b] Sergiy Minko *[a,b,c] and Vladimir Reukov*[a]

Received 18th May 2025,
Accepted 5th August 2025

DOI: 10.1039/d5nr02078f

rsc.li/nanoscale

The rapidly growing demand for cell manufacturing and *in vitro* tissue fabrication has led to the development of various technologies for biomimetic artificial extracellular matrix (ECM), including three major materials: hydrogels, fibrous scaffolds, and decellularized tissues. The latter two materials are closer to the biomimetic goal of replicating natural ECM. The scalability of the scaffolds made of decellularized tissues is limited. The development of 3D fibrous ECM is at the initial stage owing to the recent advantages of novel nanofiber spinning technologies. These novel technologies brought about simultaneous control over a range of critical characteristics, such as fiber diameter, length, material, draw ratio, spacing, and alignment into well-controlled 3D constructs. There is still a long way to go in designing 3D fibrous scaffolds based on cell response studies. The primary objective of this review is to provide an analysis of the recent progress in novel nano- and microfiber spinning methods and uncover their potential for precise fiber alignment into 3D structures.

1. Introduction

One-dimensional nanomaterials with a diameter of ~50–5000 nm from various natural and synthetic polymers are commonly referred to as polymeric nanofibers.[1] The unique set of structural, mechanical, and biochemical qualities of nanofibers includes a large surface-to-volume ratio, tunable topography, high tensile strength while maintaining mechanical flexibility, surface adaptability to functionalization, and fiber scaffold porosity.[2,3] In combination with the capacity to manufacture 3D-network architectures, the above characteristics define a broad scope of biomedical applications for nanofibers for tissue engineering,[4,5] wound dressings,[6,7] controlled drug delivery systems,[8,9] nanofilters,[10,11] *etc*. Over the past few decades, biocompatible 3D nanofiber scaffolds (3D NFS) have gained considerable interest in regenerative medicine due to their ability to mimic the natural ECM and replicate the features of human tissues at different scales, guiding cell adhesion, differentiation, and migration.[12–14]

Today, developing materials with ECM-mimicking microstructure is the leading research objective of tissue engineering[15] and cellular agriculture.[16] The complex and inhomogeneous architecture of ECM has been broadly studied in various tissue types (bone[17] and cartilage,[18] tendon and ligament,[19,20] vascular,[21] skin,[22] *etc*.) to establish the role it plays in cell behavior and tissue recovery processes. Represented by interwoven protein fibers, such as fibrillar collagen and elastin, the ECM forms a natural network with a hierarchical structure at nano- and microscale levels.[23] Decellularized nanofibrous scaffolds have recently attracted significant research attention because of their remarkable cytocompatibility and biodegradability, enhancing tissue regeneration. These natural polymeric biomaterials obtained by the removal of cellular contents using physical (freeze–thawing, perfusion decellularization, high hydrostatic pressure treatment), chemical (ionic, non-ionic, zwitterionic detergent), and enzymatic (proteases and nucleases) methods preserve the cytoskeletal structure of ECM to ensure a suitable microenvironment for cell adhesion and proliferation.[24] The facilitated transport of nutrients and air to the cells is enabled through the native fibrous network with a pore size optimal for a specific cell type. Thus, decellularized ECM (dECM)-based scaffolds have been introduced in skin,[25] bone,[26] nerve,[27] vascular,[28] liver,[29] and kidney tissue engineering.[30] Despite the successful application of decellularized tissues,

[a]*Textiles, Merchandising and Interiors, University of Georgia, Athens, GA 30605, USA. E-mail: reukov@uga.edu; Tel: +1864-643-7937*
[b]*Nanostructured Materials Laboratory, Department of Chemistry, University of Georgia, Athens, GA 30605, USA. E-mail: sminko@uga.edu; Tel: +1706-338-1319*
[c]*CytoNest, Inc., 425 River Road, Athens, GA 30602, USA*

these materials have limitations caused by restricted availability (human or animal donors) and structural and dimensional characteristics. Along with naturally derived materials that mimic a favorable non-immune environment with native 3D architecture, artificial scaffolds made of synthetic or natural polymer fibers and their fabrication techniques are being actively explored.[31–33] Attempts to provide a material with biomimetic characteristics are generalized by the fundamental idea of controlling the structural features of fibers, such as diameter, spacing, alignment, and interconnectivity, at the nanoscale. Accordingly, nanofibers that comprise the native matrix structure are the key to understanding why the development of nanofibrous materials is crucial in biomedical research.

The next step to improving nanofiber scaffold manufacturing methods is controlling fiber alignment during deposition. Electrical, mechanical, and magnetic forces have been applied for fiber drawing to fabricate well-structured patterns of nanofibers aligned along a particular direction.[34,35] Highly aligned nanofiber scaffolds exhibit enhanced mechanical strength and guide cell adhesion, migration, and growth. Kular *et al.*[36] underlined two forms of communication between cells and matrix: focal and dynamic adhesions. Focal adhesion characterizes the behavior of cells on stiff substrates, while dynamic adhesion occurs in cell migration processes on a soft basal surface. The 3D structure of ECM offers an additional direction for cell–matrix and cell–cell interactions, cell migration, and morphogenesis. Cell–ECM interactions are enabled in all three directions, thus modulating mechanical signals to cells similar to natural tissues. Therefore, 3D NFS appears to be a more efficient cell culture platform than conventional 2D substrates.

Growing interest in polymeric nanofibers for biomedical purposes has led to the invention of numerous spinning and non-spinning fiber fabrication techniques. Among non-spinning techniques commonly used in research works, it is necessary to highlight such methods as 3D printing,[37–39] phase separation,[40,41] template-assisted synthesis,[42,43] and self-assembly.[44,45] Despite the broad representation of non-spinning fiber production methods in the literature and the relative success of their application, these approaches do not fully ensure flexibility for making nanofibers with desired diameter, interfiber distance, alignment, and other physical and structural properties. Moreover, these methods have limitations for large-scale manufacturing in the industrial sector.

The electrospinning (ES) method and its variations became the gold standard of nanofiber fabrication and replaced most conventional non-spinning techniques for producing fibrous medical supplies.[46–48] Several nanofiber fabrication principles, alongside ES technology, have been implemented in the production of nanofibers. The common mechanism for fiber formation across different spinning methods involves the extraction of polymer solution or melt from a nozzle, followed by the drawing of the fiber. This process is similar to traditional melt and dry spinning methods used to produce commodity fibers with diameters ranging from 10 to 100 μm. However, manufacturing nanofibers with specific structural properties necessitates a careful approach for adjusting the fiber-drawing force, which is crucial in preventing fiber rupture. As a result, nanofiber spinning technologies depend on sensitive devices that utilize electrical, magnetic, mechanical, and gravitational forces. To fabricate highly aligned arrays of fibers, specialized machine designs are required to accurately position the fibers. These important considerations form the basis of this review, which examines four groups of fiber-spinning techniques: ES, magnetic field-assisted spinning, mechanical drawing, and gravitational drawing.

Once the desired 2D fiber alignment and spacing are achieved, a 3D structure can be fabricated using a bottom-up additive manufacturing (AM) method by engineering a multi-layer stack. The multi-layer architecture is typically obtained by either combining several 2D sheets or depositing the next 2D aligned structure on top of the base (Fig. 1). Alternatively, top-down and bottom-up lithography technologies can be used to generate 3D microstructures.[49] However, such technologies are too slow and costly for various applications.

To summarize the above, this study prompts us to look into recently discovered ways to construct nanofiber-based 3D scaffolds as bioactive substrates to support cell growth. Special attention is devoted to the comparative characteristics of different spinning techniques used to fabricate nanofiber sheets with high alignment and adjustable structural parameters. In this review, we evaluate nanofiber fabrication methods in light of possibilities to control fiber diameter, spacing, and alignment that, together with the mechanical properties of the fiber material, will define the viscoelastic properties of the scaffold – the critical characteristic of the artificial ECM.[50,51]

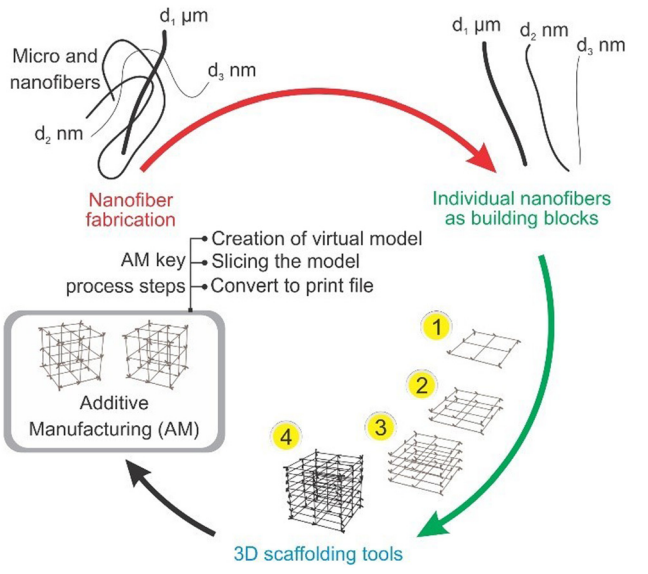

Fig. 1 The illustration of fibers as building blocks in the construction of 3D NFS by AM techniques.

2. Nano- and microfiber fabrication techniques

Nanofibers can be fabricated with a variety of structural features, including smooth, hollow, porous, core–shell, ribbon, and beaded morphologies. Most drawing techniques produce fibers with a high aspect ratio (length-to-diameter ratio), where the length typically ranges from a centimeter to a meter and the diameter varies between a few microns to several tens of nanometers. These techniques aim to utilize various biocompatible and biodegradable polymers, each possessing unique structural and mechanical peculiarities. The following subsections cover the most promising nano- and microfiber-drawing methods introduced in recent research, starting with broadly discussed ES and moving on to novel approaches of mechanical and gravitational drawing. These innovative methods are designed to ensure tunable fiber characteristics (diameter and interfiber distance) and controlled fiber deposition onto collecting substrates. We structured this part of the methods' review based on the origin of the external force (electrical, magnetic, mechanical, and gravitational) applied to pull the fiber from droplets of polymer solutions or melts. For that reason, the current section discusses four major groups of spinning techniques: ES, magnetic field-assisted spinning, mechanical, and gravitational drawing.

2.1. Electrospinning

Fiber fabrication techniques have been explored for almost a century with the advent of ES for textile yarn production.[52] Despite the development of novel nanofiber fabrication methods, major research and commercialization efforts are still invested in ES-based techniques, which are the most broadly used for tissue engineering applications, with several thousand publications in recent years. Thus, over 16 000 scientific articles on "*Electrospun nanofibers for biomedicine*" were reviewed from Scopus and Web of Science databases between 2010 and 2024.

The design of the apparatus for artificial polymeric thread production developed by Formhals in 1934 opened the opportunities for utilizing electrostatic forces to draw the fibers out of solutions and melts.[53] A conventional ES setup comprises four major components – a high-voltage source, a syringe pump with a vessel tube, a spinneret or a needle with a blunt tip (nozzle), and a grounded collector for fiber deposition. A nozzle extruding a polymer solution is connected to a high voltage, and a fiber-collecting substrate is connected to the ground at a distance (Fig. 2A). During the process of ES, the droplet of polymer solution or melt extruded from the needle undergoes charging. The repulsive electrostatic forces generated between identical surface charges overcome surface tension and let the charged droplet deform into a Taylor cone (Fig. 2B), from which a charged jet is ejected. Further transformation of the jet includes its extension along a straight line followed by the whipping motion stage that occurs due to electrical bending instability. When the finer diameter of the jet is achieved, it solidifies on the collector, forming semi-crystalline fibers. A study[48] accurately describes the main ES stages with theoretical models of the process. Fibers of a few tens to hundreds of nanometers in diameter can be fabricated and collected as fibrous mats on different types of collectors.

As discussed in ref. 56, the ES process and the features of deposited fibers are affected by multiple parameters that can be divided into three groups: polymer solution/melt properties, ES process parameters, and environmental parameters. The first group, or so-called material attributes, involves molecular weight and concentration of polymer and thermodynamic quality of the solvent, resulting in the solution's non-Newtonian viscosity, conductivity, surface tension, and solvent evaporation rate. According to ref. 57, the efficient production of nanofibrous mats is typically achieved from polymer solutions with a concentration of <20 wt%, surface tension of <50 mN m^{-1}, and dynamic viscosity of ~1 Pa s. The voltage applied for fiber drawing, the distance between the droplet and collector, the solution pumping rate, and the type of spinneret (rotating ball, cylinder, disc, spiral coil spinnerets, *etc.*[58]) and collector are related to the process parameters. Temperature and humidity are traditionally referred to as environmental variables. All the above parameters must be optimized for the fiber fabrication.

The ES technique gained commercial success due to the simplicity and scalability of the process. However, several tech-

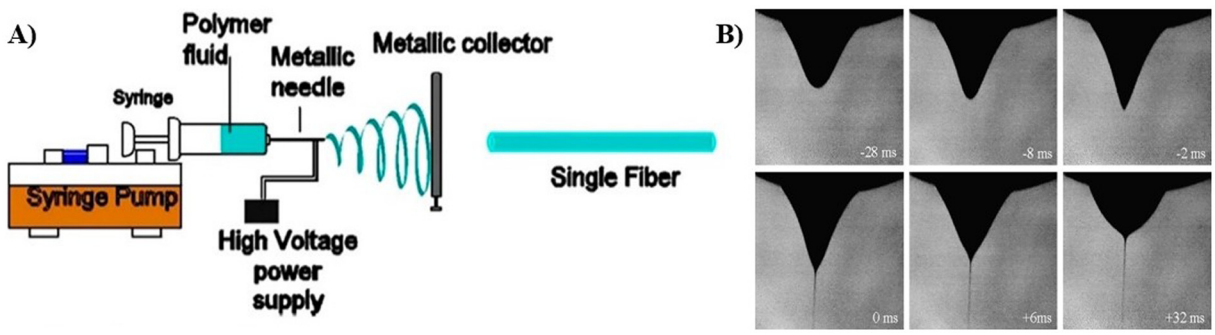

Fig. 2 (A) Conventional ES setup. Adapted from ref. 54 with permission from American Chemical Society, copyright 2021; and (B) the evolution of polyethylene oxide (PEO) droplet shape during the ES process. Reproduced from ref. 55 with permission from Elsevier, copyright 2008.

nological features impose limitations on the use of ES. Thus, applying high voltage (usually several tens of kV) is considered the key drawback of the technique, which necessitates adherence to specific safety protocols and procedures and hence affects scalability. Additionally, producing nano- and microfiber mats with a high degree of fiber alignment using standard ES techniques remains challenging without specific modifications to the setup. In the absence of such enhancements, electrospun non-woven fiber sheets typically exhibit a disordered fiber arrangement, which is suboptimal for tissue engineering applications requiring highly aligned scaffolds. Such alignment is critical for ensuring efficient and, ideally, well-regulated nutrient transport within a 3D-structured scaffold. Several modified ES techniques have been developed over the past decade to overcome these challenges. For instance, different configurations utilizing a rotating drum (mandrel) instead of conventional collectors in combination with either a single needle[59,60] or two needles with opposite voltages[61] have been introduced to improve fiber deposition in a controlled manner. A relatively straightforward approach for enhancing filament alignment during the ES process – commonly referred to as gap ES – involves the use of two negatively charged parallel plates (or analogous configurations) that facilitate a back-and-forth jet motion. This parallel plate collector setup has been shown to support the formation of meter-long, aligned nanofibers, as the positively charged polymer jet is directed across the intervening gap.[62,63] Despite these innovations, controlled interfiber distance and 3D scaffolding remain a challenge due to inherent instabilities of the solution jets.

The ES techniques applied for nanofibrous mat production are commonly divided into two categories – needle-based (capillary) and needleless (capillary-free) ES.[57,64] The proposed classification with several popular ES techniques is presented in Table 1.

2.1.1. Coaxial electrospinning. The development of coaxial ES techniques enables new methods for drug and gene delivery using nanofibers. These techniques are used to create core–shell fibers, which allow for a controlled release of the components contained within the nanofibers. In this approach, the outer polymeric layer (shell) protects bioactive molecules loaded in the core from direct interaction with the environment, helping to preserve their functionality and prolong their release. Genes, proteins, growth hormones, antibiotics, and other bioactive components have been effectively embedded in the internal layers of the core–shell materials using coaxial ES.[56]

Unlike a conventional ES setup where the polymer solution is delivered through a single hollow needle, coaxial ES involves two or more concentric hollow needles, making it a form of multi-jet ES. Each needle is connected to the syringe pump, which controls the flow rate of the solution. When the inner (core) and outer (shell) fluids reach the end of the needle, the shell fluid surrounds the core fluid, forming a complex Taylor cone in the presence of an external electric field.[48] A setup for coaxial ES is shown in Fig. 3A and B.

Table 1 Different configurations of ES based on the overall design modification and nanofiber collector type[57]

	Design modifications	Variations based on the shape of the collector
Needle-based (capillary) ES techniques	Multiaxial ES	Frame collector
	- Coaxial	Water bath grounded collector
	- Triaxial	Two-ring collector
	Multi-jet ES	Patterned electrodes
	Porous hollow tube ES	Parallel conducting collector
	Magnetic field-assisted ES	Rotating thin disk
	Gas-assisted/gas jet ES	Rotating wire drum collector
	Conjugate ES	Rotating frozen mandrel
	Centrifugal ES	Microfiber-assisted rotating collector
	Near-field ES	Rotating mandrel collector with parallel conducting
Needleless (capillary-free) ES techniques	Bubble/blown bubble ES	Rotating tube collector with knife-edge electrodes
	Two-layer fluid ES	Sharp pin with a rotating mandrel
	Splashing ES	Rotating drum collector
	Melt differential ES	
	Gas-assisted melt differential ES	
	Rotary cone ES	
	'Nanospider' technology (rotating roller ES)	
	Edge ES	

For example, to fabricate a multifunctional scaffold for skin regeneration, core–shell PGS/PCL nanofibers were fabricated *via* coaxial ES and loaded with platelet-rich plasma.[67] A study[68] reports the development of electrospun poly(L-lactide-*co*-ε-caprolactone) (PLCL)/poly(vinyl alcohol) (PVA) scaffolds for the treatment of diabetic wounds, enabling a dual delivery of bioactive molecules to target a lack of vascularization at wound sites and infection. A water-soluble PVA-based core was used to incorporate vascular endothelial growth factor (VEGF), while a less degradable PLCL-based outer layer was loaded with amoxicillin to prevent wound infections. Additional surface modification with amoxicillin-loaded liposomes was applied to ensure an immediate burst release of biomolecules, making this type of material a triple-layered drug delivery system.

Another example of core–shell nanofiber dual functionality is demonstrated by Anjum *et al.*[66] In this research, the authors focused on osteogenic–osteoclast coupling process regulation in bone regeneration. PLGA/PCL nanofibers were obtained by coaxial ES and loaded with hydroxyapatite (PLGA shell) and alendronate (PCL core) (Fig. 3C). The presence of hydroxyapatite, a major inorganic constituent of natural bone tissue, promotes the osteogenic differentiation of bone mesenchymal stem cells, and alendronate, known as an active compound

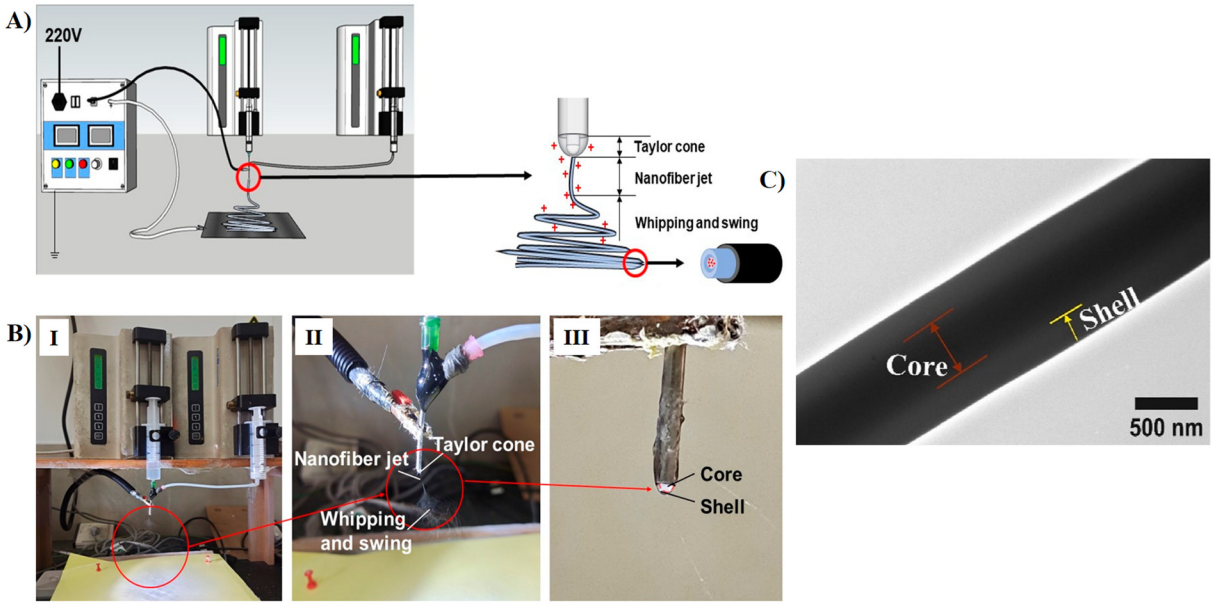

Fig. 3 (A) Schematic diagram of a simple coaxial ES setup illustrating core and shell fluids in a coaxial configuration; (B) actual coaxial ES setup: I – overall image of spinning, II – needle point magnification diagram of spinning process, III – core (white) and shell (transparent) fluids at the exit of the needle. Figures (A) and (B) have been reproduced from ref. 65 with permission from Multidisciplinary Digital Publishing Institute, copyright 2023; (C) transmission electron microscopy (TEM) image illustrating the distinctive core–shell structure in the poly(lactic-*co*-glycolic acid) (PLGA)/PCL nanofibers with a diameter of 479 ± 163 nm. Hydroxyapatite and alendronate were embedded in the PLGA shell and PCL core, respectively. Adapted from ref. 66 with permission from Elsevier, copyright 2024.

against osteoporosis, inhibits osteoclastic activity when released from the PCL core. The integration of coaxially electrospun nanofibers with 3D printing technologies was successfully demonstrated in work[69] devoted to the fabrication of biphasic scaffolds for the treatment of osteochondral defects. In contrast to ref. 66, PLGA, in combination with hydroxyapatite or chondroitin sulfate, was used to create the core layer, while protoporphyrin IX-loaded gelatin formed the shell.

The production of fibers by coaxial ES imposes additional conditions on both the properties of core–shell fluids and the technological parameters of the device. Thus, the immiscibility of the fluids is a major factor when generating the core–shell jet in the electric field. It should be taken into account to prevent unfavorable mixing or inversion of two liquids. In addition to solution viscosities defining the effective ES process, core and shell fluids should possess similar dielectric properties to ensure a similar electric force. Among the technological parameters, the characteristics of the needles and the flow rates of fluids play a key role in enabling precise core–shell fluid delivery.

2.1.2. Multi-jet electrospinning (MJES). The multi-jet or multi-needle ES is a technique aimed to increase the productivity of fiber manufacturing by replacing a single hollow needle in the conventional setup with an array of hollow needles arranged into various geometric patterns (such as linear, square, circular, elliptic, hexagonal, *etc.*).[70–72] Another method of implementing MJES involves placing a grounded electrode near the single needle, which creates a strong electric field gradient, inducing multiple jets from the droplet.[48] However, in both scenarios, the process is accompanied by high jet instability due to additional Coulombic repulsion between the jets. Increasing fiber production rates has been a significant challenge, as traditional ES approaches typically offer a flow rate of ~1–5 mL h^{-1} (0.1–1 g h^{-1} by fiber weight), as reported elsewhere.[73] For this reason, it is crucial to develop various MJES configurations to improve scalability.

An important advantage of this method is the ability to create complex multi-component structures by using two or more different polymer solutions simultaneously. As mentioned in subsection 2.1.1., coaxial electrospinning can be seen as a subtype of MJES, which allows for the production of multifunctional core–shell structures applied in drug and gene delivery systems.

MJES techniques involving various spinneret configurations (*e.g.*, number of needles, distance between the needles, overall geometric arrangement, *etc.*) have been successfully implemented in recent research works.[74–76] SalehHudin *et al.*[77] conducted a thorough study on how voltage and needle configuration impact the electric field and jet characteristics in a model system with linearly arranged needles. By varying the number of needles (up to five), inter-needle spacing, and voltage, the authors determined the optimal conditions for uniform electric field distribution and stabilization of the neighboring jets. In another study,[76] the researchers proposed an innovative gas-assisted MJES setup for producing PEO nanofibers. A novel 19-needle spinneret with a hexagonal needle arrangement was used to boost nanofiber production to 0.618–0.712 g h^{-1}. To enhance the ejection of multiple jets

and reduce electrostatic interplay between them, the authors introduced sheath gas into the system at various pressures. Scanning electron microscopy (SEM) results demonstrated that applying sheath gas led to fiber thinning. At the highest pressure of 50 kPa, the nanofiber diameter was reduced to 250–375 nm, compared with 325–475 nm for nanofibers obtained without sheath gas.

The multiple-jet approach offers unique opportunities, such as increased fiber production, fabrication of multicomponent matrices, and the ability to create complex structures. However, the main challenges of the method associated with high bending instability and irregular jet paths remain unresolved. These challenges require precise regulation of spinneret design and the electric field in the system, which significantly restricts the large-scale application of the method in regenerative medicine.

2.1.3. Near-field electrospinning (NFES). The distance between the tip of the spinneret and the collector is a critical operational parameter in ES, as it influences both fiber diameter and alignment by preventing the jet from undergoing significant bending instability in the electric field. Generally, shorter tip-to-collector distances result in larger fiber diameters, as the jet is not sufficiently thinned prior to deposition. Although fundamental factors such as solution viscosity, polymer molecular weight, and the applied voltage primarily govern fiber thickness, the shortened jet trajectory and limited solvent evaporation inherently reduce the extent of jet stretching in the electric field, determining the final fiber diameter. Notably, shorter working distances provide greater precision in arranging fibers over a surface area. Most ES techniques utilize standard tip-to-collector distances of 10–20 cm (far-field mode), which requires the application of high voltages, typically in the range of 10–50 kV.[78,79] Reducing the tip-to-collector distance to 500 μm–5 cm helps to lower working voltages to less than 1 kV, resulting in the near-field ES.[80] The images illustrating the reduced tip-to-collector distance in the NFES setup are provided in Fig. 4A.

A detailed review of NFES progress[80] summarized the advancements in NFES techniques used for manufacturing PEO fibers. The authors acknowledged that using a movable collector or a movable spinneret allows for the direct deposition of fibers in different patterns. Thus, by decreasing the collector speed from >0.35 to 0.05 m s^{-1} while maintaining a constant tip-to-collector distance of 1 mm and voltage of 1.7 kV, it becomes possible to achieve fibers shaped in straight lines, wavy lines, single- or multi-circle coils (as shown in Fig. 4B–D).[81] The general concept for controlling specific nonwoven patterns involves matching the speed of the jet motion with the relative speed between the collector and the spinneret. A particularly clear example of how a short tip-to-collector distance can decrease the required voltages is given elsewhere.[82] The study examined the impact of voltage on the diameter of PEO fibers during the NFES process carried out with a tip-to-collector distance of 1 mm and a collector moving speed of 0.04 m s^{-1}. Therefore, the voltages used in this study ranged from 200 V to 600 V, which is a significant voltage reduction compared with far-field ES. A near-field direct-writing ES with a moving collector plate was utilized to create well-aligned composite collagen/PCL-based wound dressings loaded with anti-infective component erythromycin.[83] The distance between the tip and the collector was 2 mm (Fig. 4E), while the voltage applied was 2 kV, and the collector speed was maintained at 0.08 m s^{-1}. In order to generate multi-layer orthogonally aligned nanofiber mats, the authors employed special grids with a 1 × 1 mm spacing (Fig. 4F). This demonstrates the effectiveness of the NFES approach in creating aligned structures.

Currently, the NFES techniques can produce thin fibrous membranes with reasonably controlled fiber spacing, orientation, and alignment. In this method, the electric field is highly concentrated between the spinneret and the collector, which helps to decrease the required voltages. Despite its progress, NFES still faces several challenges. These include the need for a controlled mechanism to optimize polymer jet deposition, inefficiency in depositing fibers in precise 3D structures, and integration issues with other micro/nanofabrication approaches for scalability. Additionally, reducing the tip-to-collector distance requires lower solution flow rates, leading to lower production rates. The smaller distance increases repulsion between forming and deposited jets, causing jet instability and hindering fiber patterning. Despite the attempts to control fiber diameter by introducing movable collectors or spinnerets, the fabricated fibers often have large diameters that may not meet the materials' requirements.

2.1.4. Stable-jet electrospinning (SJES). In the previous section, the NFES technique was described as a way to reduce the chaotic whipping of the jet by decreasing the distance between the tip of the spinneret and the collector. However, spinning at reduced tip-to-collector distances often results in poorly dried and coalesced fibers. A promising ES approach called stable-jet ES is designed to address the limitations of NFES. It enables the production of ultrafine linearly aligned micro- and nanoscale fibers. The term introduced by Zhang *et al.*[84,85] refers to the method of stabilizing the jet length by improving the polymer–solvent interaction throughhigh polymer concentration and molecular weight. Thus, using high molecular weight components provides sufficient viscoelasticity and chain entanglement in the spinning solution, which forms the core concept of SJES.[86]

The SJES method was applied in recent research works.[87–89] One study[89] suggested the approach to produce highly aligned high-strength silk fibroin/PEO microfibers for induced pluripotent stem cell-derived mesenchymal stem cell (iPS-MSC) culture. A high molecular weight PEO (M_w > 5000 kDa) was used to increase control over the whipping instability during the SJES process (Fig. 5). The ultrafine poly(L-lactide acid) (PLLA) fibers with a tensile strength of up to 122.5 ± 6.29 MPa were collected on a rotating cylinder electrode using the SJES technique.[90] The process effectiveness and variables were assessed based on different viscosity average molecular weight PLLA (M_w = 100–700 kDa). In addition, the mechanism of SJES for poly(methyl methacrylate) (PMMA) ribbon-shaped microfi-

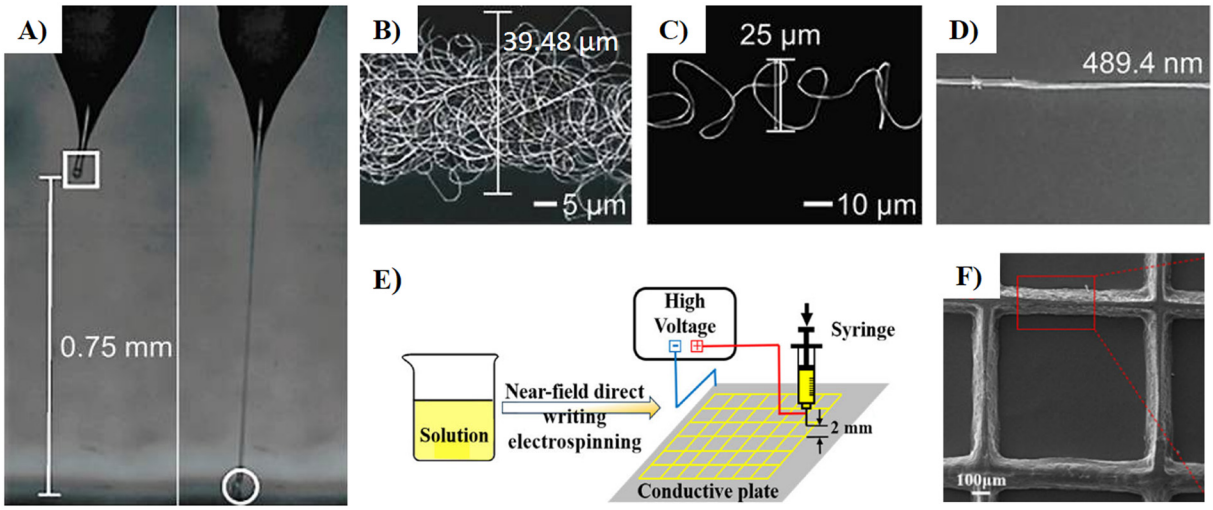

Fig. 4 (A) Motion process of charged PEO in NFES at an applied voltage of 1.7 kV and tip-to-collector distance of 1 mm recorded using a high-speed camera; (B–D) SEM images of nanofibers deposited on a planar silicon substrate during NFES at a collector moving speed of (B) 0.03 m s^{-1}, (C) 0.20 m s^{-1}, and (D) 0.36 m s^{-1}. Figures (A–D) have been adapted from ref. 81 with permission from Institute of Physics Publishing, copyright 2010; (E) scheme of experimental NFES setup; (F) SEM image of well-aligned composite collagen/PCL fibers loaded with erythromycin. Figures (E) and (F) have been adapted from ref. 83 with permission from Multidisciplinary Digital Publishing Institute, copyright 2024.

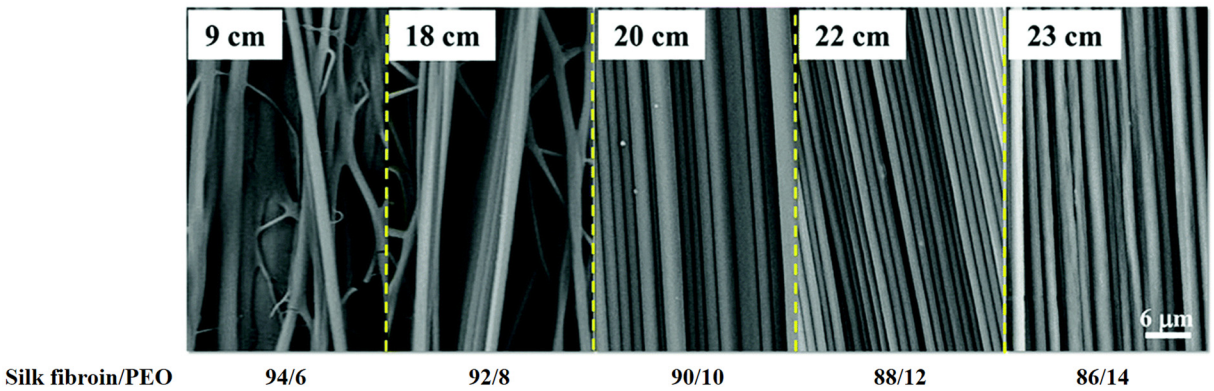

Fig. 5 Morphologies of well-aligned silk fibroin/PEO fibers with different polymer contents collected at different stable jet lengths using SJES. The operating voltage, pumping rate, and rotating electrode speed are 8.5 kV, 0.2 mL h^{-1}, and 700 rpm, respectively. Reproduced from ref. 89 with permission from Royal Society of Chemistry, copyright 2018.

bers deposited on a rotating drum collector was studied in another work.[86] The authors utilized high molecular weight PMMA (M_w = 500 kDa) in the concentration range of 5–40 wt% in different solvents to determine the optimal conditions for fiber spinning.

This simple ES modification allowed for the rapid fabrication of microfiber scaffolds with controlled fiber spacing, alignment, and porosity. While SJES is effective for certain applications, its limitation lies in the minimum achievable stable fiber diameter, which is several micrometers.[91]

2.1.5. Needleless electrospinning. 'Nanospider' technology. There has been a lot of interest in needleless ES techniques following the discovery of the roller ES. This method, developed by Jirsak *et al.*,[92–94] is commonly known as the 'Nanospider' technology (ELMARCO s.r.o., Czech Republic) and has been a breakthrough in ES for producing nanofibers over the past 15 years.

The 'Nanospider' technology utilizes rotating rollers and cylinders as carrying electrodes. The rotating roller is typically located at the bottom, and the grounded electrode-collector is positioned at the upper part of the ES apparatus. The polymer solution is placed onto the top roll surface of the bottom electrode (or the roller is partially immersed in the reservoir with the polymer solution), leading to the upward movement of the jets when the electric field is applied.[56] The scheme of the roller ES is given in Fig. 6A. The roller ES is considered a needleless version of the MJES, as multiple Taylor cones are induced from the surface of the carrying electrode with the polymer solution, resulting in increased productivity. Different variations of the apparatus exist, but most use high voltages of

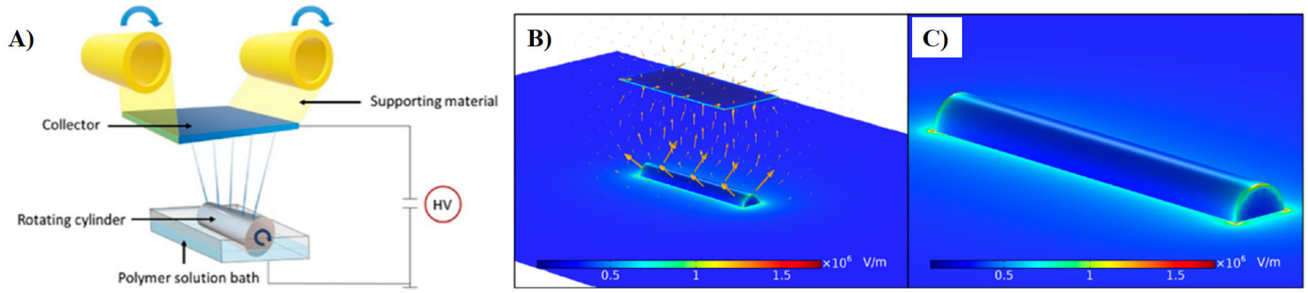

Fig. 6 (A) Schematic representation of the 'Nanospider' technology setup with a cylinder electrode, (B) simulation of the cylinder and collecting plate configuration, (C) simulation of the electrostatic charge distribution on the electrode. Figures (A–C) have been adapted from ref. 95 with permission from Multidisciplinary Digital Publishing Institute, copyright 2021.

several tens of kilovolts and standard electrode-to-electrode distances of 10–20 cm for fiber production. Moreover, the electric field around the elongated electrode is concentrated mostly at the edges, as confirmed by analytical simulations (Fig. 6B and C).[95] The nozzle parameters (diameter, length, *etc.*) are not as important in such a system, but the amount of polymer solution introduced to the electrode needs to be adjusted.

In a study,[96] a system utilizing a bottom-up jet movement was implemented to create non-woven mats of PVA containing microscale particles of calcium salts for culturing dental pulp stem cells (DPSCs). The 'Nanospider' NS LAB 200S laboratory unit (ELMARCO, Czech Republic), with a fixed electrode-to-electrode distance of 16 cm, was used to produce nanofibers with diameters in the range of 190–530 nm. The authors noted that the presence of inorganic inclusions resulted in an increase in operating voltages from 27 to 42 kV, in contrast to pure PVA-based nanofibers. A recent research paper[97] describes the application of another NS LAB 500S (ELMARCO, Czech Republic) 'Nanospider' device to manufacture drug-loaded PLLA/PVA/chitosan nanofibrous mats for use as wound dressings. In this study, the authors utilized an increased operating voltage of 80 kV at a fixed electrode-to-electrode distance and electrode rotation rate. Therefore, the 'Nanospider' technology is not exempt from one of the key drawbacks of ES – the requirement for high voltage during the process, which necessitates the implementation of additional safety measures when operating the setup. The method's simplicity for producing fibers does not offset the high production costs and prevents large scalability.

2.1.6. Melt electrospinning. The methods outlined in the previous subsections are commonly used ES modifications designed to enhance productivity and/or tailor the structural and geometric characteristics of the resulting fibers for biomedical research. These modifications, involving but not limited to coaxial, multiple, and stable jets, have been successfully tested in solution-based systems and have the potential to be adapted for non-solution systems, such as melts.

Melt electrospinning has long been discussed in the literature alongside ES from polymer solutions; however, significantly less research has been conducted on this technique until recent innovations emerged. This lack of focus can be attributed to two main factors: (1) the cost of establishing a melt ES device is somewhat higher than that for a solution ES setup, as the apparatus requires a heating reservoir (supply zone); and (2) the fibers produced by melt ES typically have greater diameters compared with those made through solution ES, primarily due to the significantly higher viscosity of polymer melts.[98] This elevated viscosity impedes the elongational and thinning forces exerted by the electric field, thereby limiting jet stretching and resulting in thicker fibers. Several research studies have demonstrated the possibility of obtaining melt electrospun fibers with submicron diameters,[99] contrasting with the second factor that hinders the widespread distribution of this technique for producing nanofiber scaffolds.

With the current trend in tissue engineering toward creating an ordered deposition of fibers, melt ES could become a valuable tool to accomplish this objective. The viscosity of the polymer melt is sufficient to suppress repulsive Coulombic charge interactions. Consequently, melt ES offers a stable flight path for the melt jet, resulting in less chaotic fiber deposition. This improved jet stability, akin to that in SJES, enhances control over fiber alignment in electrospun meshes. Additionally, eliminating solvents from the ES process is a significant advantage of this method compared with solution ES. Often, the solvents used in solution systems can be toxic to cells and tissues. Toxic solvent residue may remain after the jets solidify during the ES process, necessitating further material post-treatment. A notable example of this issue is the use of acidic solvents (primarily, acetic and trifluoroacetic acids) in ES from chitosan-based systems.[100] Thus, melt ES becomes an alternative, environmentally friendly technology that processes biocompatible polymers 'as received' from the supply zone. These important aspects, along with the potential to apply the technique to non-soluble polymers such as polypropylene (PP), polyethylene, polyphenylene sulfide, *etc.*, have piqued research interest in melt ES for producing commercial biomaterials.[99]

In the electrostatic field, the behavior of the melt jet follows the same principles as in conventional solution ES, with one exception: the final step does not involve solvent evaporation.

Instead, the jet crystallizes on the collecting substrate due to the temperature gradient, leading to the formation of amorphous or semi-crystalline materials. The reduction of bending instabilities significantly minimizes the stretching that the jet undergoes before crystallization. Moreover, because there is no thinning from solvent evaporation, the fiber diameters produced in this process are larger compared with those created through solution ES, often reaching tens of micrometers. The detailed description of the major melt ES steps, including jet thinning, jet quenching, and fiber crystallization, is well-documented in a study,[98] along with the corresponding theoretical models and equations.

A melt ES apparatus typically consists of three main zones: a supply zone, a high-voltage zone, and a fiber collection zone. The supply zone that delivers the molten polymer to the jet initiation point uses various driving mechanisms, including air pressure, syringe pumps, screw extruders, and mechanical feeding mechanisms. The polymer moving through the supply zone can be pre-heated to its melting point by direct electrical resistance sources, heated circulating fluids, or lasers. The jet initiation point serves as the entry to the high-voltage zone for the ES process. It can involve various systems, such as needle-based and needleless systems, gas-assisted melt ES designs, and other configurations reducing the diameter of the collected fibers. The collectors in the fiber collection zone may be stationary or moving, such as *x*–*y* stages and rotating collectors, to create desirable fiber patterns and perform so-called direct writing (Fig. 7B). These directly written arrays with high fiber alignment can be easily assembled into 3D constructs using AM technologies.

The melt ES technique offers the potential to create ultrafine fiber arrays that can be collected over extended periods. This makes it an appealing method for the commercial production of materials intended for biomedical applications. However, only a limited number of commercially available polymers have been thoroughly investigated. The materials that have been studied include commonly used polymers for tissue engineering, such as PCL,[101] PLGA,[102] poly(lactic acid) (PLA),[103] as well as poly(ethylene glycol)-*block*-PCL/PCL (PEG-*b*-PCL/PCL), PEG-*block*-PCL, PLA/PEG and other blends.[98] Several groups of polyolefins and polyamides, which are difficult to dissolve in common solvents and require high processing temperatures, were successfully utilized in melt ES. Thus PP, known for its exceptional toughness and resistance to various chemical solvents, was melt electrospun in one study.[104] Additionally, polyurethane (PU) elastomers, frequently characterized by the presence of hard aromatic units, were successfully melt electrospun both individually and in blends with low melting point polymers like PCL.[105] According to the analysis presented in ref. 98, fewer than 30 polymers have been thoroughly studied in the melt ES process, highlighting the need for further research on this method.

2.2. Magnetic field-assisted techniques

Several ES techniques have been optimized by introducing an external magnetic field to the collector region to improve the properties of fabricated materials, particularly controllable fiber diameter and alignment. The application of the external magnetic field in ES technologies (MF-ES) is discussed in several works[106–108] aimed at obtaining oriented fiber mats. As a rule, two magnets at a certain distance are mounted in the conventional ES setup at the collector region so that the charged jets experience a radial Lorenz force in the magnetic field and stretch across the gap of two opposite poles. The magnetic field gradient controls the diameter and direction of the deposited jets.[108]

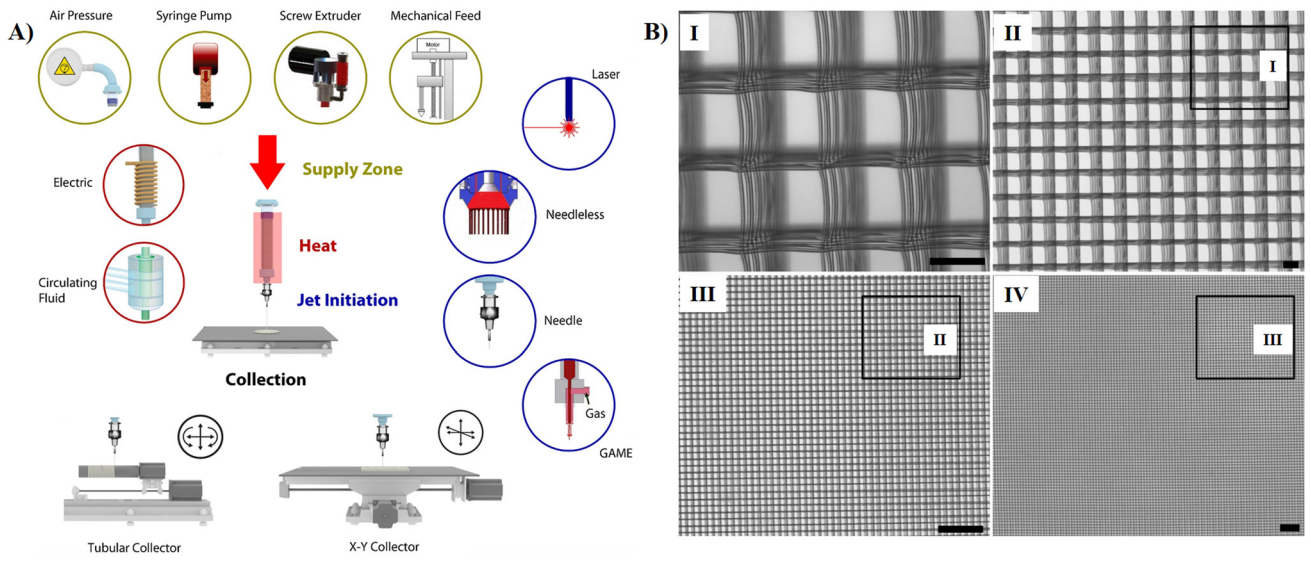

Fig. 7 (A) Schematic of the melt ES configurations reported in the literature, (B) stereomicroscope images of a PCL scaffold fabricated using a melt ES technique. Electrospun fibers are aligned orthogonally with interfiber distance of 150 μm in both axes: scale bars for I–II and III–IV are 100 μm and 1 mm, respectively. Figures (A) and (B) have been adapted from ref. 98 with permission from Elsevier, copyright 2016.

Another concept of fiber drawing in the presence of the external magnetic field is based on mixing polymer solutions with so-called ferrofluids, colloidal dispersions of stabilized magnetic nanoparticles. Metallic (Co)[109,110] and magnetite (Fe_3O_4) nanoparticles[111,112] coated with stabilizers are typically used as dispersion phases and dissolved in aqueous or organic solvents to create ferrofluids. Tetramethylammonium hydroxide and fatty acids are commonly used stabilizers that prevent nanoparticles from aggregation.[113,114]

Magnetospinning (MS), developed by Tokarev *et al.*,[115,116] is a new technique for producing ultrafine nano- and microscale fibers. It utilizes the external magnetic field and ferrofluids containing magnetite nanoparticles with an average diameter of 9 ± 1.5 nm. In their study,[116] the nanoparticles obtained by a co-precipitation method were stabilized by oleic acid or trisodium citrate and loaded to the solutions of polystyrene (PS), PCL, and PMMA in chloroform, or aqueous PEO solutions at various mass fractions. The scheme of the apparatus for MS with fiber-drawing steps is presented in Fig. 8. As described in this study, the magnetic field is generated by a permanent magnet fixed on a rotating circular stage with a controlled angular velocity. A syringe needle with polymer solution is placed at a certain distance to the magnet, and a syringe pump supplies the solution. Due to the magnetic force, the droplet starts to deform at a critical distance between the needle and the magnet, and as the stage continues to rotate, the droplet jumps toward the magnet, and the fibers are drawn. The magnetic field force was shown to generate enough stretching force to overcome the surface tension. Similar to ES, the evaporation of the solvent occurs during fiber drawing. The fibers are deposited on the collector located on the opposite side of the stage.

One of the advantages of MS, along with fiber alignment and low energy consumption, is that the dielectric properties of the solution do not affect fiber formation. No specific criteria are required for the dielectric constant of the solvent and polymer, and a broader range of materials can be utilized for fiber manufacturing. MS enables the fabrication of continuous fibers with diameters ranging from 50 nm to tens of micrometers. It is important to note that despite the benefits

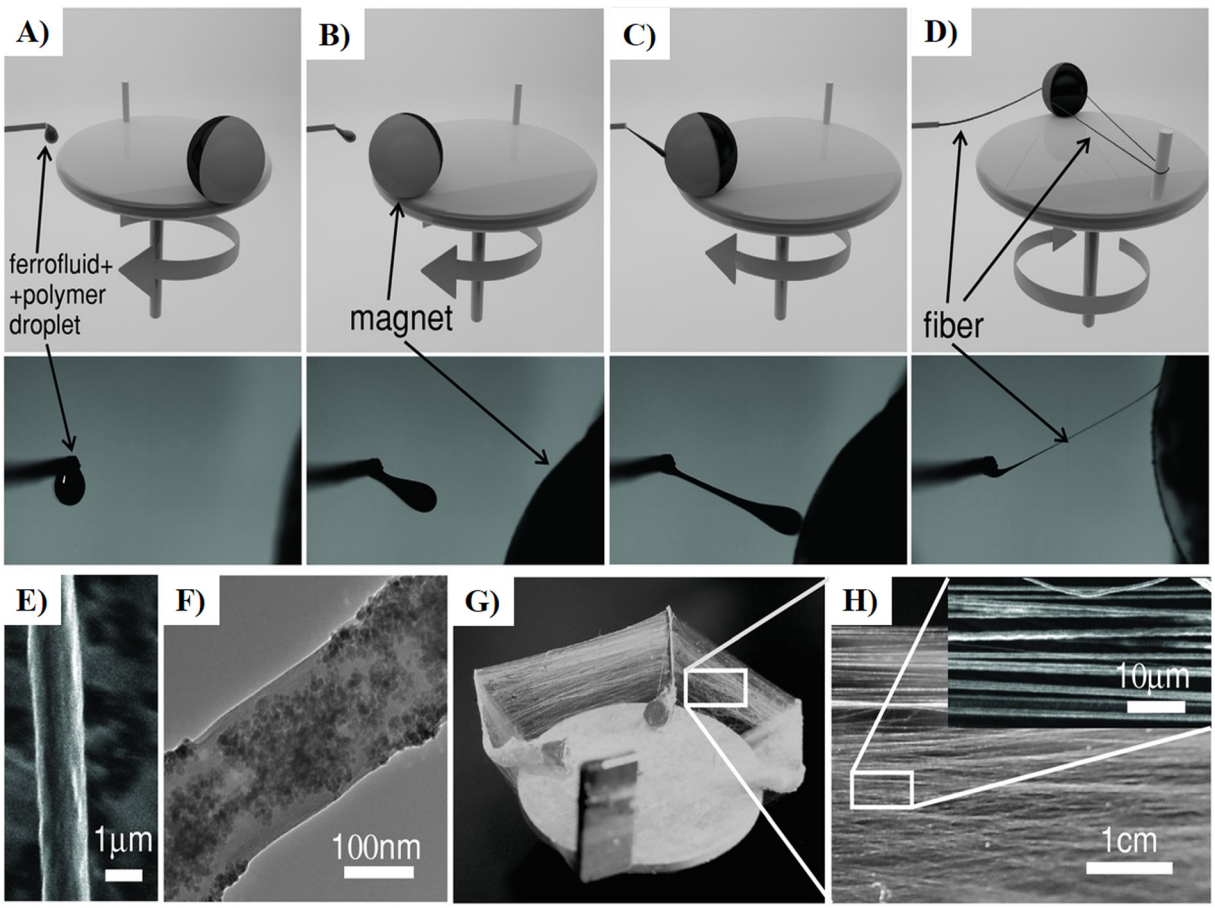

Fig. 8 The magnetospinning setup and fiber-drawing process: (A) the formation of the solution droplet at the end of the needle, (B) the deformation of the droplet surface in the presence of the permanent magnet (gray and black colors represent the north and south poles of the magnet, respectively), (C) the formation of the liquid bridge between the needle and the magnet, (D) the drawing of fiber, (E) and (F) SEM and TEM images of PCL fiber obtained using the magnetospinning setup, (G) and (H) photograph of the aligned PCL fibers deposited on the collector within 5 minutes at the stage rotation rate of 500 rpm. Figures (A–H) have been reproduced from ref. 116 with permission from Wiley-Verlag Chemie, copyright 2015.

of the method compared with ES, the preparation of ferrofluids is an additional and sometimes laborious step in MS. Usually, the magnetic particle size and shape must be optimized for the efficient spinning process, which requires careful control during the colloidal synthesis of nanoparticles. The studied fibrous materials are designed to create biocompatible and biodegradable matrices supporting cell growth. However, even small fractions of inorganic constituents, such as iron oxides and metal particles, can adversely affect the cell–matrix interactions or contaminate the culture media.

Unfortunately, very few research works have focused on developing magnetic field-assisted techniques for controlled fiber manufacturing. The invention of MS in 2015 did not result in further significant achievements in this area. However, the goal of eliminating the external high-voltage power supply from the spinning setup and reducing the whipping instability during fiber formation has led to the development of several new devices using the magnetic field to produce highly aligned fiber patterns. Thus, Zhang *et al.* introduced a portable magnetic melt spinning (MMS) setup with a moving collecting platform to fabricate submicron PS fibers in various patterns.[117] The MMS prototype is illustrated in Fig. 9A.

Like MS, the MMS uses a ferrofluid consisting of Fe_3O_4 nanoparticles at a doping degree of 5 wt% to initiate the formation of a liquid bridge between the droplet and the collector. In the suggested apparatus design, the strong magnet is located under the moving collecting platform, and several synchronous motors adjust the platform and nozzle positions. Fig. 9B shows the simulation of magnetic field distribution between the tip and collector, as well as the forces acting on a melt droplet. In this work, the researchers managed to obtain sinusoidal fibers with an average diameter of 900 nm and their orthogonally laid strips, as illustrated in Fig. 9C and D. Even though the technique utilizes melts to produce fibers and, therefore, contains a chamber with a temperature-controlling device, it can be easily adapted for drawing fibers from polymer solutions.

2.3. Mechanical nanofiber drawing

In recent years, tissue engineering research has introduced state-of-the-art methods for fiber fabrication involving mechanical drawing with no external fields. These methods offer an advantage for manipulating fibers of various lengths and diameters with only mechanical forces acting on polymer solutions with adjustable viscosities. The solution parameters associated with responsiveness to electric and magnetic fields become eliminated, and the techniques can be used with a variety of natural and synthetic polymers. Utilizing mechanical forces instead of electrical or magnetic ones is expected to significantly reduce production costs and simplify operational protocols during fiber manufacturing.

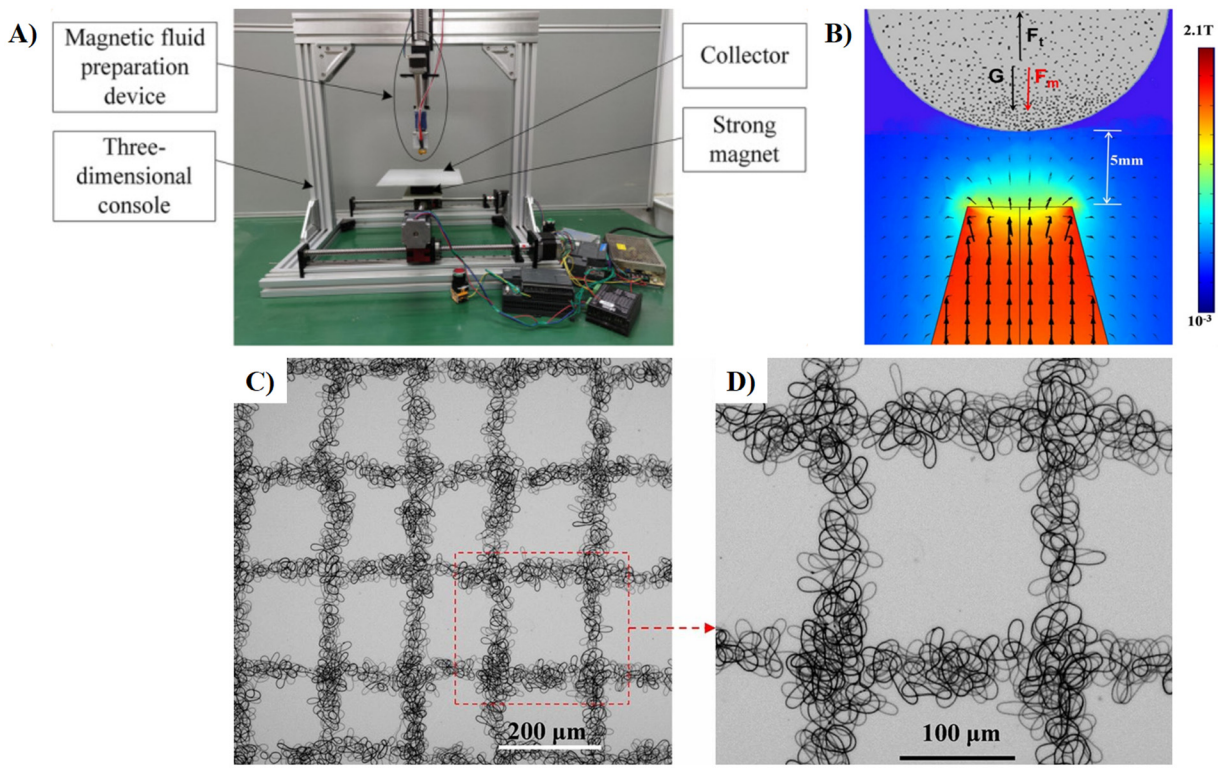

Fig. 9 (A) The image of a homemade MMS prototype; (B) the simulation of the magnetic field in the region of 5 mm outside the nozzle tip: G, F_t, and F_m correspond to gravitational force, surface tension, and magnetic force, respectively; (C) and (D) SEM images of patterned architecture of PS fibers at different magnifications. Figures (A–D) have been adapted from ref. 117 with permission from Nature Portfolio, copyright 2021.

2.3.1. Track-spinning (drawing) (TS). A good example demonstrating the application of mechanical stretching force for fiber drawing from polymer solutions is a hand-drawing method[118] developed from observing everyday activities. The polymers used for the hand-drawing do not need to possess any specific electrostatic properties, and the process efficiency depends mainly on the non-Newtonian viscosity of the solutions. The drawing of uniaxially aligned fibers from a polymer solution by the hand-drawing method is shown in Fig. 10A.

Track-spinning is a straightforward single-step method for fabricating nano- and microscale polymer fibers developed based on the hand-drawing concept. A design of a track-spinning apparatus suggested by Jao and Beachley[119] includes two oppositely rotating tracks with the upper ends pushed against each other and the lower ends widened to stretch the fibers (Fig. 10B, C and E). The polymer solution is extruded at the joined ends, creating a coat on the tracks. Thus, the solution on the tracks is subjected to a mechanical force. As the tracks continue to move down and away from each other, single or multifilament arrays of fibers are gradually drawn from the coat. The drawing of fibers in a controlled manner can be achieved by adjusting such process parameters as the angle of the tracks, the vertical collection distance (the distance between the joined ends and the collection tray), and the track speed. In the work,[119] a successful application of this method for fiber drawing was demonstrated based on poly(vinyl

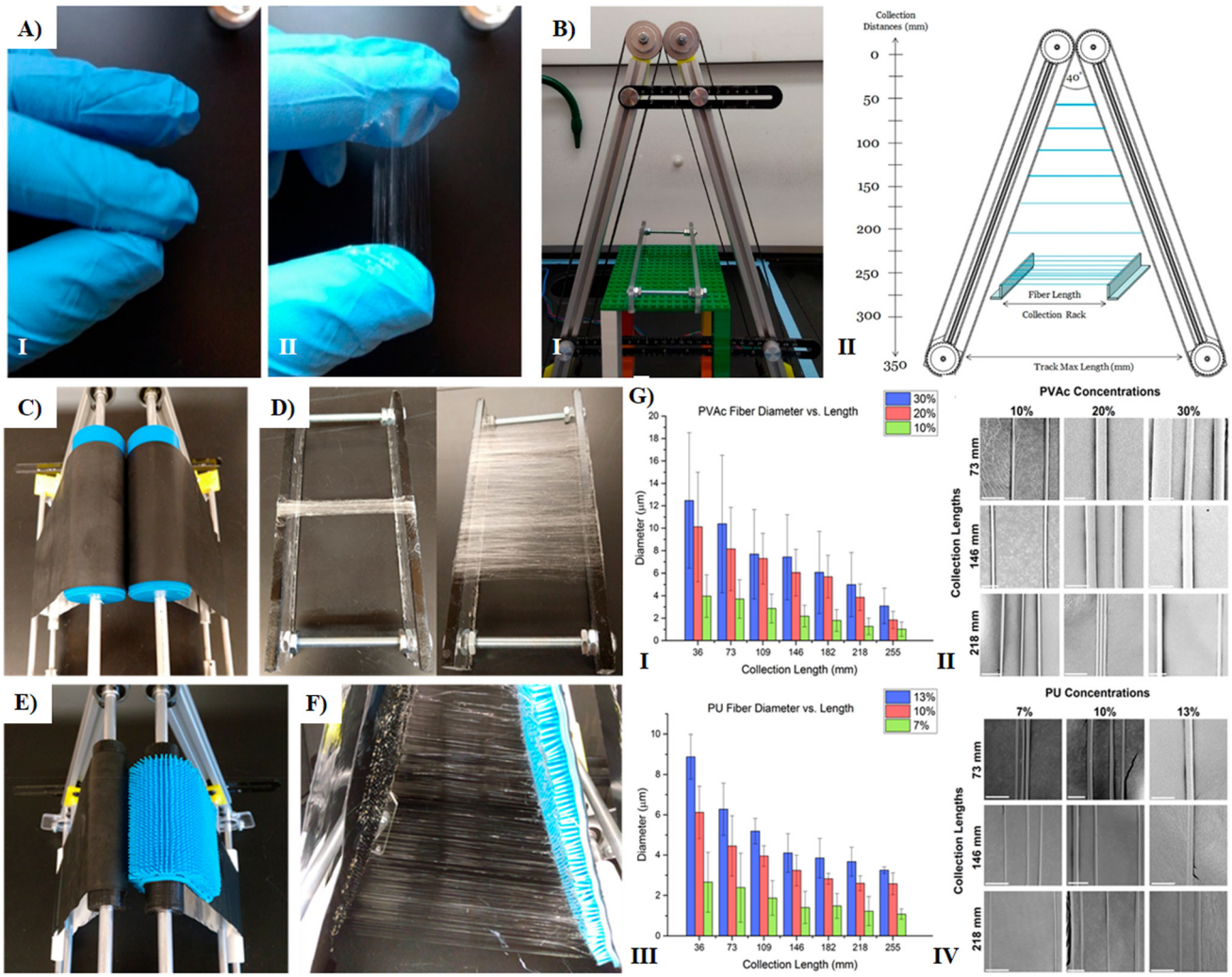

Fig. 10 (A) Photograph of the hand-spinning process: a droplet of polymer solution is fixed between the thumb and index finger (I), polymer solution is drawn producing uniaxially aligned fibers (II); (B) track-spinning apparatus: photo of a homemade track-spinning device (I), schematic illustration of the apparatus with process parameters used in the study (II); (C) photo of a 3D spinning system developed based on 2D track-spinning; (D) photo of the aligned PS fibers collected using the 3D and 2D spinning systems during the same amount of time; (E) photo of the 3D track-spinning system for patterned fiber drawing; (F) stretching of the aligned poly(vinyl acetate) fibers using the patterned 3D track-spinning system; (G) track-spun fiber characterization: diameter–collection length relationship for poly(vinyl acetate) fibers (I), SEM images of poly(vinyl acetate) fibers obtained at different collection lengths from the solutions of various concentrations (SEM scale bar = 20 μm) (II), diameter–collection length relationship for PU fibers (III), SEM images of PU fibers obtained at different collection lengths from the solutions of various concentrations (SEM scale bar = 20 μm) (IV). Figures (A–G) have been adapted from ref. 119 with permission from American Chemical Society, copyright 2019.

acetate), PU, and PS solutions, as well as PCL melts. During the experiment, the angle of the tracks and the draw rate were fixed at 40° and 6.26 mm s^{-1}, respectively, while the vertical collection distance was varied to investigate its effect on the geometric characteristics of fibers. It is possible to reach nanoscale fiber thickness by tuning the process parameters or post-drawing the fibers to greater lengths, as was reported by the authors. The post-drawing of fibers to the length of 255 mm reduces fiber diameter to 450 nm. The fibers obtained by track-spinning and their SEM images are shown in Fig. 10D, F and G.

The track-spinning technique produces highly aligned arrays of nanofibers with controlled length and diameter, but the control of the interfiber spacing is limited. The fixation of fibers at both ends and using various collectors allow for further fiber assembling into 3D structures.

2.3.2. Centrifugal spinning (CS). A modified centrifugal spinning, also known as CS-Forcespinning, was first reported by Sarkar *et al.* in 2010 and further commercialized by FibeRio Technology Corporation.[120,121] CS technology features low cost and high yield and has no complex technical requirements for the production of nonwoven fabrics on a lab or industrial scale. The working principle of the method is based on centrifugal force generated from high-speed rotation. The centrifugal force can stretch the polymeric jets from highly concentrated solutions and depends on the rotational (angular) speed, spinning head dimension, and the weight of the spinning dope.

The current CS devices consist of three main parts – a syringe fixed along the rotating axis, a spinning head (or rotating reservoir) made of plastic or metal, and a motor equipped with a speed-controlling system. A scheme of a simple CS device is shown in Fig. 11A. The CS design has multiple variations, including multi-jet configuration with symmetrically set syringes, needleless, or airflow-assisted CS. Additionally, the combination of ES and CS, resulting in electro-centrifugal spinning, is currently being studied to integrate the advantages and overcome the limitations of both techniques (Fig. 11B).[121]

According to the Google Scholar database, over 18 000 scientific articles mentioning centrifugal spinning (including those devoted to commercialized Forcespinning technology) have been published over the past decade. The CS technique has been applied to many biocompatible polymer solutions and melts to fabricate highly efficient materials for tissue engineering[122–124] and drug delivery.[125–127] For instance, nanofiber scaffolds based on PCL and osteogenic supplements were prepared using a forcespinning device at a rotational speed of 10 000 rpm and studied in combination with human bone marrow-derived mesenchymal stem cells to confirm long-term drug-releasing properties.[127] A recent work[125] reported another successful application of CS for drug delivery system fabrication. PLLA microfibers functionalized with anti-inflammatory drug ketoprofen were obtained at the rotational speed of 18 000 rpm and studied toward the mouse preosteoblast cell line (MC3T3-E1). Control over a microscale fiber diameter by regulating the rotational speed was demonstrated in the study[128] of composite sodium alginate/Antarctic krill protein fibers fabricated *via* modified CS at relatively low speeds of 100–300 rpm. Numerous conductive and non-conductive materials can be force-spun using the CS method, and the production rates can be remarkably improved by increasing the rotational speed of the spinning head.[129] Most examples proved the ability to adjust fiber diameter at the nano- and microscale, but the alignment and interfiber spacing remain random (Fig. 11C).

The geometry and morphology of the force-spun fibers depend on the speed of rotation, air perturbation, device vibration, tip configuration, tip-to-collector distance, *etc.*, which frequently leads to beaded fiber morphologies,[131] as illustrated in Fig. 11D.

2.3.3. Spinneret-based tunable engineered parameter (STEP) technique. Most nano- and microfiber spinning methods discussed previously, except for a few modified ES techniques, do not ensure precise control over fiber alignment and interfiber spacing. Until recently, the alignment and interfiber spacing remained random, although fiber diameters could be adjusted by managing three groups of parameters (see section 2.1. Electrospinning). The geometry of fiber patterns is crucial in cell mechanobiology, as it guides cell adhesion and orientation along the individual filaments. To address this, several new mechanical drawing techniques that utilize stepper motor systems have been developed. Among these techniques, spinneret-based tunable engineered parameter (STEP) technology and touch-spinning are two competitive methods relying on similar fiber-drawing principles.

The STEP technology was first introduced by Nain *et al.*[132] as a pseudo dry-spinning technique for producing high-aspect-ratio fiber arrays in aligned configurations with controlled diameters of 50–500 nm. The experimental setup design contains a micropipette spinneret with a diameter of 20–100 μm located perpendicularly to the collecting substrate. The substrate of a given shape (rectangular, cubic, spherical, *etc.*) is positioned on a DC motor, which in turn is mounted onto a motorized micropositioning stage. Thus, the substrate performs both rotational (V_r) and translational (V_t) motions, as illustrated in Fig. 12A. The process starts when a droplet of polymer solution extruded from a micropipette is brought in contact with the rotating substrate, whose angular and vertical speeds are regulated by the motorized system. As the substrate rotates, the droplet volume stretches into a filament and is further deposited on the substrate in its solidified form. The vertical translation of the substrate ensures continuous fiber deposition in a parallel configuration with controlled interfiber spacing, which can be easily seen from the example of a rectangular frame used as the collecting substrate. Thus, along with rheological (solution) parameters, such process parameters as rotational and vertical speeds become dominant in the STEP technique. Single and multiple layers of fiber arrays can be fabricated using the discussed principle.

Despite the simple concept of accurate control over fiber spacing, the STEP method has not received widespread distribution in scaffold manufacturing, and literature reports are

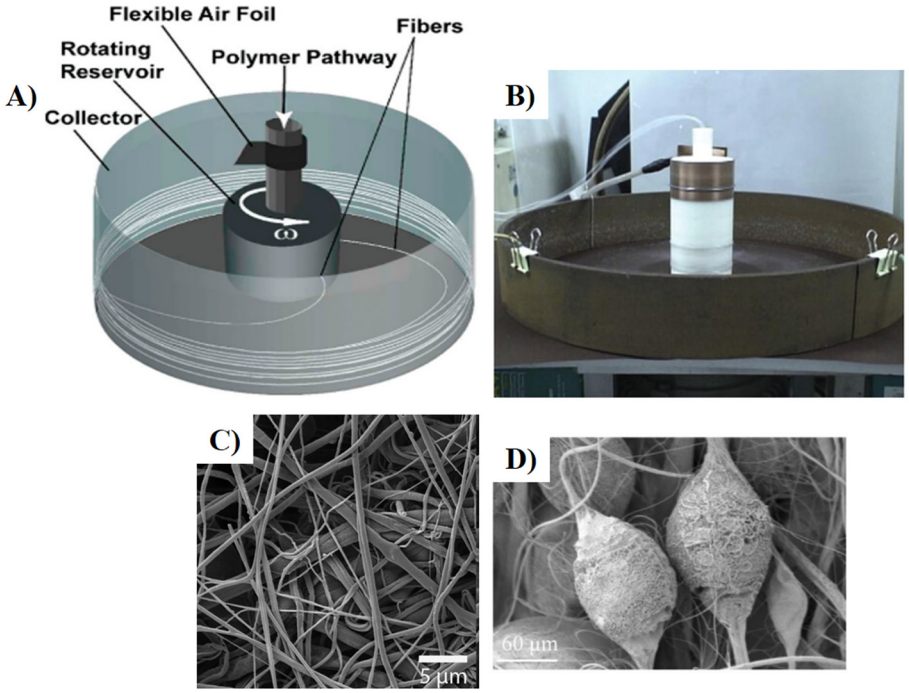

Fig. 11 (A) Schematic illustration of CS apparatus. Adapted from ref. 130 with permission from Multidisciplinary Digital Publishing Institute, copyright 2023; (B) photo of the electro-centrifugal spinning apparatus. Adapted from ref. 121 with permission from Wiley-Verlag Chemie, copyright 2023; (C) SEM image of the chaotic PCL nanofibers. Adapted from ref. 127 with permission from Royal Society of Chemistry, copyright 2018; (D) SEM image of force-spun fibers with beaded morphology. Adapted from ref. 131 with permission from Multidisciplinary Digital Publishing Institute, copyright 2022.

limited to a few[132–136] about the apparatus design and STEP-spun scaffold application for cell cultures. Initially applied to the fabrication of PS and PMMA nanofiber arrays on planar and non-planar substrates (Fig. 12B), the STEP method was further implemented by the same research group to obtain aligned multi-layer structures consisting of three different polymers – PS, PMMA, and PU.[136] Thus, the authors developed six-layer scaffolds with orthogonally aligned micro- and nanofiber arrays using STEP-spun fibers of various diameters as 1D building blocks, as illustrated in Fig. 12C. In detail, PS fiber arrays with a diameter of ~5 μm and interfiber spacing of 100 μm were used to construct the first and second layers, PMMA fibers of smaller diameter (~1 μm) and interfiber spacing (50 μm) were deposited on top of the lower PS layers as the third and fourth layers, and nanoscale PU fibers (~300 nm) with the spacing of 10 μm formed the two upper layers of the scaffold. In addition, the study describes a way of controlling C2C12 mouse myoblast cell/organoid geometries and focal adhesion sizes by varying divergent angles between adjacent fibers (Fig. 12D). A dry-spinning technique utilizing a screw slide platform and a rotating substrate was used in the recent study performed by Gu *et al.*[137] to manufacture microscale PCL fibers (~8 μm) with a sparse and dense arrangement. In this work, parallel fiber patterns with the interfiber spacing of 161.3 ± 22.9 μm and 19.1 ± 12.5 μm were prepared. Moreover, the fabrication of dry-spun fiber arrays is only a small part of comprehensive research aimed at establishing the effect of fiber diameter and spacing on bone marrow stem cell proliferation and osteogenesis. The influence of these key parameters is studied separately, and criteria for cell cross-adhesion between adjacent fibers are provided based on two groups of materials (sparsely and densely arranged) obtained by ES, dry, and wet spinning.

In ref. 138, a shear force spinning device was developed for the lab-scale fabrication of sparse PS fibers with a tunable average spacing of 230 ± 40 μm. The proposed device follows the STEP technology principles and does not require highly advanced automated micropositioning systems. Additionally, the authors assessed primary solution and process parameter relationships, such as the draw-down ratio (DDR), the entanglement concentration (C_e), and the capillary number (Ca).

The STEP technique is promising for obtaining nano- and microfiber arrays with tunable geometric characteristics. A simple concept of mechanical stretching combined with versatile motorized systems makes it attractive in bioscaffolding. For the first time, fiber diameter, fiber alignment, fiber spacing, and assembling of fibers of different diameters in a 3D construct were precisely controlled.

2.3.4. Touch- and brush-spinning (ThS and BS). A touch-spinning method, introduced by Tokarev *et al.* in 2015,[139] is another method based on the mechanical drawing principle. Similar to the STEP technology discussed above, it employs rotational and translational motions of apparatus parts to deposit aligned nano- and microfibers with controlled dia-

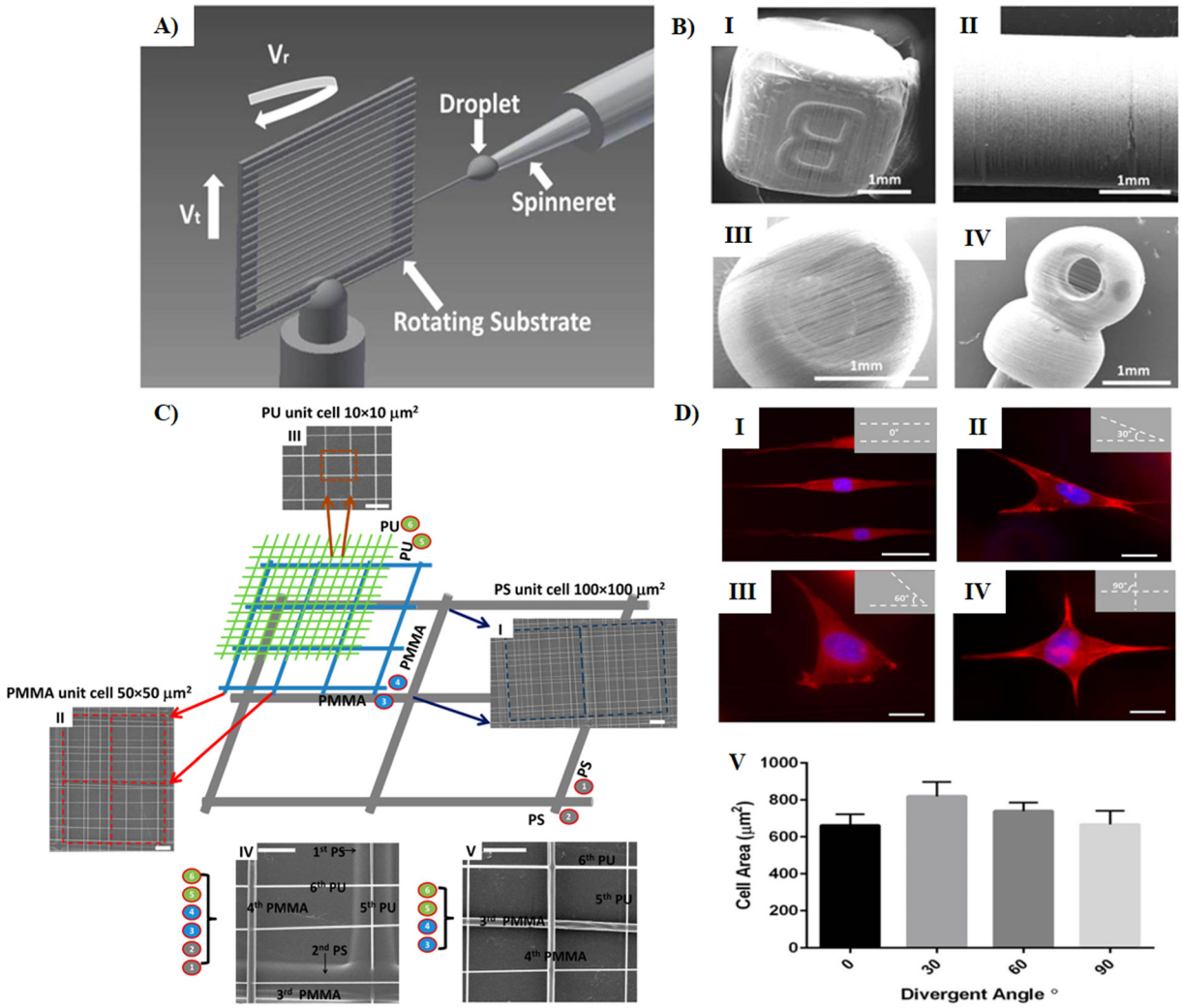

Fig. 12 (A) Illustration of mechanical fiber drawing in STEP technology with rectangular substrate performing rotational (V_r) and translational (V_t) motions; (B) STEP-spun fibers collected on the substrates of different shapes – cubic (I), cylinder (II), spherical (III), and shape-assembled (IV); (C) six-layer hierarchical assembly of fiber arrays. Inserts I–III correspond to PS, PMMA, and PU unit cells, respectively, inserts IV and V show the bottom-up deposition sequence (SEM scale bar = 10 μm); (D) fluorescent images of C2C12 cell geometries on PS fibers (diameter ~300 nm) aligned at 0° (I), 30° (II), 60° (III), and 90° (IV) (scale bar = 20 μm) with cell spread area calculated as a function of divergent angles (V). Figures (A–D) have been adapted from ref. 136 with permission from American Chemical Society, copyright 2014.

meters and interfiber spacing. In contrast to the STEP apparatus, the touch-spinning apparatus uses a rotating spinneret, which is a rod mounted on a rotating disk. The revolving rod comes periodically in contact with the polymer solution, and the drawn fibers are deposited on the collector, which is located at the disk center. In contrast to the STEP method, each disk revolution leads to drawing a new fiber. The fiber production increases with the number of rods mounted on the disk. Depending on the device design, the collector is either mounted on the rotating disk or connected to the step motor and placed above the disk. In the latter case, the translational motion of the collector in the direction orthogonal to the disk plain is used to control interfiber spacing. The touch-spinning process scheme and a particular device prototype are illustrated in Fig. 12A–C and D, respectively.

The mechanism of the fiber drawing is analogous to the mechanism of the STEP technique. The initial apparatus design involved a glass rod of a specific diameter (ranging from 0.3 mm to several mm) attached to a rotating stage. This rod is brought into contact with a droplet of polymer solution pushed out from a syringe tip using a pump. After the rod 'touches' the droplet, it creates a liquid bridge and stretches the fiber along the stage diameter while rotating. The fibers solidify upon solvent evaporation. In order to prevent the deposition of the polymer on the rod, the surface of the rod can be coated to reduce its wettability. Fig. 12D demonstrates a device with a metal spinneret rotating around the collector mounted in the middle of the device chamber. The collector moves up and down at a programmed speed. Thus, the rotational and vertical speeds and major solution parameters,

such as concentration and viscosity, are explored to control fiber characteristics and alignment.

The touch-spinning method enables precise control over fiber diameter in the 40–5000 nm range and allows for the production of parallel fiber arrays with interfiber distances varying from ~10 μm to several centimeters. The fiber production rates can be significantly improved by introducing multiple syringes into the system, resulting in multi-jet touch-spinning. Coaxial needles can be used in this method to spin core–shell fibers. Additionally, this method is highly scalable, inexpensive, and compatible with AM technologies for constructing multi-layer structures, similar to those shown in Fig. 12C. The touch-spinning apparatus can produce meter-long fiber layers, depending on the size of the collecting frame, which allows for building up large 3D scaffolds.

The effectiveness of touch-spinning in producing aligned fiber patterns with uniform diameters was initially demonstrated using simple biocompatible polymers (PEO, PCL, and PVA) widely employed in biomedicine for constructing surgical threads, wound healing membranes, or tissue substitutes. It is important to note that the high degree of orientation and alignment of touch-spun fibers has created opportunities to study cell cultures that require directed growth along the substrate elements. Neurons and smooth muscle cells are examples of such cultures. Thus, one study[140] compares electrospun and touch-spun PCL nanofibers, showing promoted neurite outgrowth of NE-4C cells on aligned touch-spun scaffolds with a fiber diameter of 431 ± 30 nm. The expression of TUJ-1, a neuron-specific protein indicating the earliest stages of neuronal differentiation, was found to be enhanced for BSA-incorporated touch-spun nanofibers. Additionally, the authors hypothesized that the combination of high elastic modulus (79 ± 11 MPa) and high crystallinity degree of touch-spun nanofibers might have influenced actin reorganization and activated GTP binding proteins, leading to guided cell neurogenesis. Recent research works[141,142] have employed touch-spinning principles to fabricate fibrous scaffolds based on PCL co-polymers and blends with other polymers. The efficiency of touch-spun multi-layer networks with a high degree of orientation has been demonstrated toward C2C12 mouse myoblast and other cell lines. Despite its potential for precise 3D cell culture applications, touch-spinning technology remains underexplored in the scientific literature, with only a few recent studies providing preliminary insights into its capabilities.[143–146]

Brush-spinning is another promising method of fiber manufacturing that builds on touch-spinning technology. It aims to improve scalability by using multiple spinnerets (filaments) in the process. The brush-spinning device, as described in ref. 139, consists of a round hairbrush with 600 filaments connected to an electrical motor to ensure rotation (Fig. 13E and F). A translational motion of the brush along the horizontal axis can also be achieved using additional motorized systems. The working solution is poured onto a Teflon film placed beneath the substrate (brush). As the substrate rotates, the filaments come into contact with the solution, leading to the stretching of fibers along the substrate. This technique has been tested on PEO, PCL, and polyacrylonitrile solutions and has demonstrated incredibly high productivity. Thus, PEO nanofibers with a diameter of 200 nm and a total length of 1700 km were produced using the round 600-filament brush (D = 6 cm) after 5 minutes of brush-spinning at a rotational speed of 3000 rpm. The arrangement of filaments in the brush creates regular fiber meshes. Therefore, both random and aligned fiber arrays can be obtained by this technique (Fig. 13G and H).

Similar to the other mechanical drawing methods, this method does not rely on the dielectric properties of materials used for fiber fabrication. The diffraction peaks for touch-spun fibers were found to have higher intensities compared with those of electrospun fibers. This suggests that touch-spun fibers have a higher degree of crystallinity. Additionally, Young's modulus of touch-spun fibers was significantly higher, again indicating that touch-spinning can achieve higher crystallinity. Furthermore, various additives can be incorporated into the polymer solution to enhance strength, conductivity, biocompatibility, and other properties.

2.4. Gravity nanofiber drawing (GD)

The design of the most recent technique, known as gravity fiber drawing (GD), was proposed by Yadavalli *et al.*[147] for the production of highly aligned 2D fiber arrays. The GD, similar to the mechanical drawing techniques discussed in section 2.3., utilizes only gravity force to form a fiber from a droplet of polymer solution, without the requirement for other external fields. This method is still very new to the field of fiber manufacturing and has great potential to become the leading AM-compatible technique, enabling precise fiber alignment. The scheme of the instrument for the gravity-drawing experiment is shown in Fig. 14A.

The GD technique involves pumping a polymer solution through a syringe needle to form a droplet. The droplet falls freely under the force of gravity and generates a meter-long single filament fiber between the needle tip and the surface of the instrument base. As the droplet falls to the base, the solvent evaporates rapidly, leaving behind a solidified polymer thread. The produced fiber can be positioned on a collector with a series of robotic arms and cut with blades, as illustrated in Fig. 14A. A fiber collector equipped with stepper motors manipulates individual fibers and aligns them on a supporting frame. It is important to note that this design allows further stretching of the fibers (cold drawing) to promote the crystallization process. Thus, the mechanical characteristics of fibers obtained by GD are assumed to be significantly influenced by the polymer crystallinity and the alignment of polymer chains in the amorphous phase.

The mentioned study[147] is the first and most illustrative example of GD application for PCL fiber manufacturing. By changing the tip-to-base distance and adjusting the polymer concentration, the authors prepared monofilament nano- and microfibers of macroscopic lengths and uniform diameters

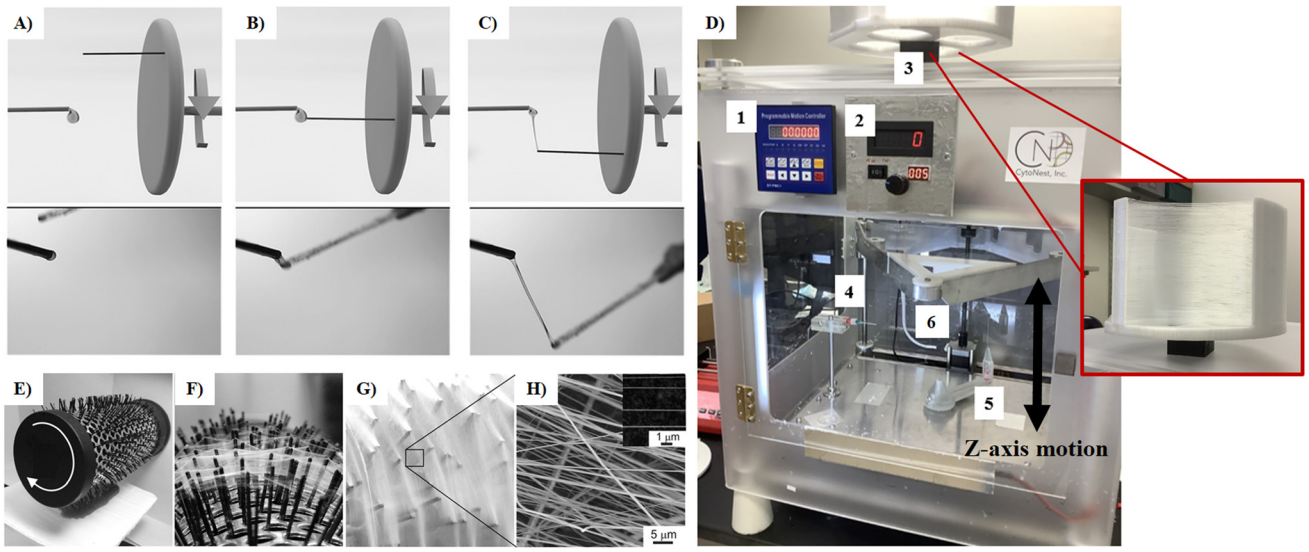

Fig. 13 Touch-spinning: (A) a glass rod on a rotating stage and a droplet of polymer solution pushed out from a syringe needle, (B) the glass rod is brought in contact with the droplet, forming a liquid bridge, (C) the glass rod continues a rotation and stretches a single fiber from polymer solution,[139] (D) modified touch-spinning device with enabled translational (*Z*-axis) motion of the substrate: 1 – stepper motor controller enabling translational motion of the substrate, 2 – spinneret controller enabling rotational motion of the spinneret around the substrate, 3 – 3D-printed substrate with collected PCL fibers (cropped image illustrates the substrate that is placed inside the chamber), 4 – a syringe connected to a syringe pump, 5 – a rotating spinneret, 6 – attachment point of the substrate. Unpublished data provided by CytoNest, Inc.; brush-spinning: (E) a 600-filament hair-brush attached to a motor, (F) and (G) PEO nanofibers collected on the brush at 3000 rpm after 1 minute and 5 minutes of spinning, respectively, (H) SEM image of randomly aligned nanofibers (cropped image demonstrates possible regular alignment of PEO nanofibers). Figures (A–C) and (E–H) have been adapted from ref. 139 with permission from Wiley-Verlag Chemie, copyright 2015.

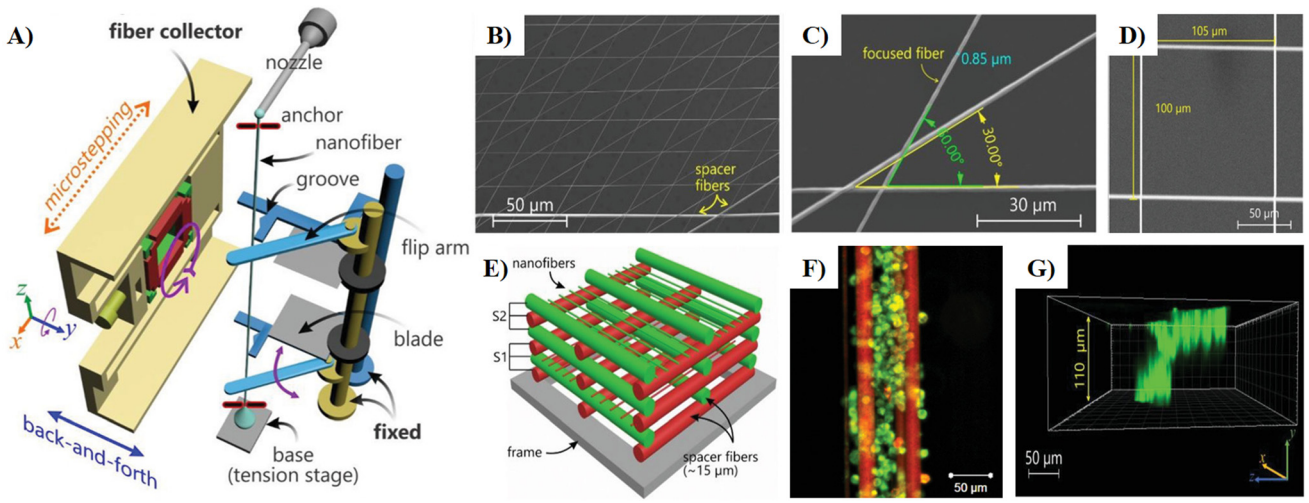

Fig. 14 (A) Scheme of the GD device; (B), (C), and (D) SEM images of 2D arrays aligned at 30°, 60°, and 90°, respectively; (E) scheme of fiber arrangement into 3D scaffold using spacer microfibers; (F) confocal microscopy image of RAW264.7 macrophages anchored to PCL fibers (cells were labeled with WGA, and fibers were labeled with red fluorescein); (G) Polaris software analysis of *z*-stack fluorescence image. Figures (A–G) have been adapted from ref. 147 with permission from Wiley-Verlag Chemie, copyright 2020.

ranging from 0.46 to 0.93 μm. As was mentioned previously, adequate and structured spacing between the fibers is essential for the appropriate cell infiltration and proliferation. Inspired by this idea, the authors fabricated 2D arrays of nanofibers with a precise interfiber spacing of 50–200 μm. The fiber collection process was demonstrated to have a reproducibility of ~95% with only a few misalignments. Another feature of this method is its compatibility with AM technologies to build up a 3D NFS by stacking 2D arrays together at a chosen angular orientation (0–360°). Fig. 14B–D demonstrates microscopy images of 2D arrays aligned at 30°, 60°, and 90°. In the study, a 3D NFS with a thickness of 0.43 mm was pre-

pared by aligning eight sets of nanofiber layers orthogonally (the interfiber spacing and layer gap were set at 50 and 45 μm, respectively). These layers can be easily combined using a series of separating spacers (or spacer fibers), as shown in Fig. 14E. Similar to touch-spinning and STEP techniques, the GD provides opportunities to overcome the fiber ordering limits present in both conventional and modified ES methods. The efficiency of the produced materials as artificial ECM-mimicking substrates was confirmed based on cell culture experiments with RAW264.7 macrophages (Fig. 14F). Thus, sufficient cell proliferation in the scaffold volume was demonstrated by confocal microscopy imaging after 5–6 days of cell growth (Fig. 14G).

Overall, the GD technique remains the youngest in the field of bioscaffolding, and many process parameters and fabricated scaffold features are yet to be explored.

3. Analysis and comparison of fiber-drawing techniques

In this section, we propose an evaluation of the nanofiber spinning methods based on two sets of criteria – one for *the scalability of the methods* and another for *the serviceability of the produced fibers and 3D fiber scaffolds*. The *scalability criteria* for each method can be assessed based on fiber production rates, costs, and compatibility with AM technologies for fabricating multi-layer 3D structures. For tissue engineering and cell culture applications, essential *serviceability criteria* include controllable fiber diameter, interfiber spacing, fiber alignment, crystallinity, mechanical strength, and micromechanical characteristics of the fiber surface. All the listed properties are known to affect guiding cell response, differentiation, and proliferation. Moreover, each specific cell line requires specific fiber properties. Thus, the optimal fiber scaffold characteristics may vary for different cell cultures.

The considerations of the nanofiber fabrication methods through the prism of *scalability* and *serviceability* related to bioengineering applications of 3D scaffolds are illustrated in Table 3.

3.1. Theory of forces acting on filaments

Theoretical aspects of fiber spinning under various conditions and an analysis of the forces acting on the filament in the quench zone were proposed by Ziabicki[148,149] in the early sixties and later discussed by Walczak in ref. 150. Using a homemade setup designed for regular wet, dry, and gravitational spinning, the authors measured the take-up forces acting on polycapronamide filaments and calculated the distribution of the forces' constituents, particularly focusing on the velocity tensor of the moving liquid. According to ref. 150, a simplified version of the force balance in the spinning system can be represented by the following equation:

$$F_e + F_g = F_r + F_i + F_s + F_a \quad (1)$$

where F stands for force, and the subscripts are: e – external, g – gravity, r – rheology, i – inertia, s – surface, and a – aerodynamic.

While the external (take-up) force typically applied by the external fields, take-up rollers, or aerodynamic jet is studied in the spinning process, other force components can be identified as shown in Table 2. Thus, along with the external drawing force F_e, the study examines the gravitational force F_g, rheological force F_r, inertial force F_i, surface tension F_s, and

Table 2 Force components in the force balance equation

Force component	Formula	Formula components
F_g (gravitational force)	$F_g = g\frac{(1-\rho_0)}{\rho} \times \cos\chi$ (2)	g – acceleration due to gravity ρ_0 – density of the surrounding ρ – density of the filament χ – angle between the filament and the horizontal
F_r (force of material deformation)	Not determined. The force can be calculated from the balance of forces for a particular spinning type	Not determined
F_i (force required for material acceleration from initial velocity)	$F_i(x) \sim \rho Q(V - \varphi_0 V_0)$ (3)	ρ – polymer density at point x Q – coefficient describing the intensity of flow (mass extruded in the unit of time) V – filament velocity at point x V_0 – initial polymer velocity φ_0 – velocity profile coefficient (the subscript '0' corresponds to a parabolic profile)
F_s (force of interfacial tension between the filament and the surrounding)	$F_s = \pi\upsilon(R_0 - R\zeta(x))$ (4)	υ – interfacial tension R_0 – initial radius of the filament R – radius of the filament at point x $\zeta(x)$ – function reflecting the change in radius of the filament with distance from the spinneret
F_a (force of external friction of the running filament in the surrounding medium)	Not fully determined. In each case, the equation derives from $dF_a = 0.5\rho V^2 \times (\pi d \times dx) \times C(\mathrm{Re})$ (5)	ρ – density of the surrounding V – filament velocity $\pi d \times dx$ – surface element $C(\mathrm{Re})$ – drag coefficient for Reynolds number

Table 3 Comparison of fiber fabrication techniques for 3D NFS manufacturing

Technique	External force (F_e)	Production		Process advantages	Process limitations	Compatibility with AM	Ref.
		Process specifications	Output				
Multiaxial ES	Electric force	Applied voltage of 10–50 kV	0.01–0.3 g per h per nozzle, up to 3.6 g h^{-1} for air-assisted systems	1. Primary method for creating core–shell fibers with high drug load and sustained release 2. Controlled fiber diameter in the range of ~10 nm to 10 μm 3. The setups can be easily portable	1. Requires high-voltage power supply 2. Complexity of multiaxial needles 3. Limited material combination 4. Requires specific dielectric properties 5. Low yield 6. Limited control over fiber spacing and alignment	Poor	154, 155 and 171
MJES	Electric force	Applied voltage of 0.9–50 kV	~30–50 times greater compared with single-needle ES	1. Increased production rates and yield 2. Allows for producing multi-material structures 3. Suitable for a wide range of materials 4. Controlled fiber diameter in the range of ~10 nm to 10 μm 5. The setups can be easily portable 6. Scalable method	1. Requires high-voltage power supply 2. Complexity of multi-nozzle systems 3. Electrostatic repulsion between jets 4. Requires specific dielectric properties 5. Limited control over fiber spacing and alignment	Poor	76, 172 and 173
NFES	Electric force	Applied voltage can be decreased to 0.2–3 kV	N/A, feed rate of 0.03–2 mL h^{-1}	1. Suitable for a wide range of materials 2. Controlled fiber diameter in the range of ~sub-100 nm to 100 μm 3. Enables precise control over fiber deposition (spacing and alignment) 4. The setups can be easily portable	1. Short tip-to-collector distance impedes fiber solidification 2. Requires specific dielectric properties 3. Presumably, low yield 4. Produces fibers with larger diameters	Moderate	82, 170 and 174
SJES	Electric force	Applied voltage of 8–20 kV	0.918 g h^{-1}	1. Enables control over fiber deposition (spacing and alignment) 2. Controlled fiber diameter in the range of sub-100 nm to 100 μm 3. The setups can be easily portable	1. Requires high-voltage power supply 2. Requires specific dielectric properties 3. Low yield	Moderate	89 and 175

Table 3 *(Contd.)*

Technique	External force (F_e)	Production		Process advantages	Process limitations	Compatibility with AM	Ref.
		Process specifications	Output				
Needleless ES	Electric force	Applied voltage of 10–50 kV	3.1 g h^{-1} (ball spinneret) 6.2 g h^{-1} (disc spinneret) 8.2 g h^{-1} (cylindrical spinneret) 90 g h^{-1} m^{-1} ('Nanospider' technology)	1. Suitable for a wide range of materials 2. Achieves fiber diameter in the range of ~10 nm to 10 μm 3. Increased production rates and yield 4. Scalable method	1. Requires high-voltage power supply 2. Expensive high-yield setups 3. Requires specific dielectric properties 4. Low fiber alignment 5. Inconsistent fiber diameters, structure, and spacing	Poor	155
Melt ES	Electric force, high temperatures	Applied voltage of up to 70 kV	Up to 75.6 g h^{-1}	1. Enables ES from materials that cannot be dissolved 2. Solvent-free, less toxic method 3. Controlled fiber diameter in the range of ~sub-micrometer to 100 μm 4. Enables precise control over fiber deposition (spacing and alignment) 5. Increased production rates and yield 6. Scalable method	1. Requires high-voltage power supply 2. Requires high temperatures 3. Difficult to remove electrostatic charge 4. Requires specific dielectric properties 5. Unsuitable for biopolymers 6. Produces fibers with larger diameters	Moderate	158, 165 and 166
MF-ES	Electric and magnetic forces	Applied voltage of 15–30 kV, magnetic field of 0.2 T	N/A, feed rate of 0.5–3 mL h^{-1}	1. Suitable for a wide range of materials 2. Achieves fiber diameter in the range of ~10 nm to 10 μm 3. Enables control over fiber deposition 4. The setup can be easily portable	1. Requires high-voltage power supply 2. Complexity of the setup and material preparation 3. Instability of magnetic field 4. Requires specific dielectric properties 5. Presumably, low yield 6. Insignificant fiber alignment	Poor	108
MS	Magnetic force	Rotation speed of 50–1000 rpm	500 nanofibers per minute at 500 rpm	1. Suitable for a wide range of materials 2. Does not depend on dielectric properties 3. Controlled fiber diameter in the range of 0.05–5 μm 4. Partially enables control over fiber deposition 5. The setup can be easily portable 6. The method can be scaled up	1. Complexity of material preparation 2. Low yield 3. Insignificant fiber alignment	Moderate	115 and 116

Table 3 *(Contd.)*

Technique	External force (F_e)	Production		Process advantages	Process limitations	Compatibility with AM	Ref.
		Process specifications	Output				
MMS	Magnetic force	Magnetic field of 0.8–1.6 T	N/A, feed rate of 0.4 mL h^{-1}	1. Does not depend on dielectric properties 2. Controlled fiber diameter in the range of ~sub-micrometer to 100 μm 3. Enables control over fiber deposition (spacing and alignment)	1. Complexity of the setup and material preparation 2. Requires high temperatures 3. Unsuitable for biopolymers	Moderate	117
TS	Axial stretching	N/A	N/A	1. Does not require external fields 2. Suitable for a wide range of materials 3. Achieves fiber diameter in the range of ~sub-micrometer to 100 μm 4. Does not depend on dielectric properties 5. Partially enables control over fiber deposition 6. The setup can be easily portable	1. Requires precise motorized systems 2. Low yield 3. Limited control over fiber diameters 4. Insignificant fiber alignment	Poor	119
CS	Centrifugal force	Rotation speed of 2000–20 000 rpm, up to 75 000 rpm (Forcespinning technology)	Up to 60 g per h per nozzle	1. Does not require external fields 2. Suitable for a wide range of materials 3. Does not depend on dielectric properties 4. Achieves fiber diameter in the range of ~sub-micrometer to 100 μm 5. Increased production rates and yield 6. Scalable method	1. Complexity of the setup 2. Expensive setups 3. Limited control over fiber morphology (beaded, thick fibers, film-like structures) and spacing 4. Low fiber alignment	Poor	121–123, 125, 130 and 141
STEP	Capillary force	Rotation speed of 550–2400 rpm	N/A	1. Does not require external fields 2. Suitable for a wide range of materials 3. Does not depend on dielectric properties 4. Enables precise control over fiber diameter (~sub-100 nm to 10 μm), spacing (5–80 μm), and alignment (0–90°) 5. The setups can be easily portable	1. Requires precise motorized systems 2. Produces small scaffolds 3. Presumably, low yield	Good	132–134 and 136

Table 3 *(Contd.)*

Technique	External force (F_e)	Production		Process advantages	Process limitations	Compatibility with AM	Ref.
		Process specifications	Output				
ThS	Axial stretching	Rotation speed of 100–2500 rpm	<0.2 g h^{-1}	1. Does not require external fields 2. Suitable for a wide range of materials 3. Does not depend on dielectric properties 4. Enables precise control over fiber diameter (40 nm–5 μm), spacing (<10 μm), and alignment (0–360°) 5. The setups can be easily portable 6. The method can be scaled up	1. Requires precise motorized systems 2. Low yield	Good	139 and 142
BS	Axial stretching	Rotation speed of up to 3000 rpm	N/A, total fiber length of 1700 km was achieved within 5 min at 3000 rpm	1. Does not require external fields 2. Suitable for a wide range of materials 3. Does not depend on dielectric properties 4. Enables control over fiber diameter (40 nm–5 μm) and spacing (down to ~10 μm) 5. The setups can be easily portable 6. The method can be scaled up	1. Requires precise motorized systems 2. Limited control over fiber diameters and structure 3. Insignificant fiber alignment	Moderate	139
GD	Gravitational force	N/A	N/A, meter-long fibers were reported	1. Does not require external fields 2. Suitable for a wide range of materials 3. Does not depend on dielectric properties 4. Controlled fiber diameter in the range of ~100 nm–100 μm 5. Enables control over fiber deposition (spacing of 20–1000 μm and alignment of 0–360°) 6. The setups can be easily portable	1. Requires precise fiber-cutting and collecting systems 2. Presumably, low production rates	Good	147 and 176

the aerodynamic drag F_a that acts on the filament in the surrounding medium.

The theory of forces acting on the filament during the drawing process was considered when developing a classification of fiber-spinning techniques for the current review. With the availability of various modern spinning techniques, we can observe that the source of the external drawing force can vary. Therefore, classifying these techniques based on the type of external force applied is useful for comparing their scalability and produced fiber performance. A comprehensive mathematical approach for determining the force components involved in both laminar and turbulent fiber motion is well documented in the works of Ziabicki. These studies serve as a key reference for further calculations related to the development of fiber-spinning machines. However, since our focus is not on the theoretical aspects of the spinning process, we will instead explore the significance of these early studies for the future of the fiber-spinning industry.

The early research on the dynamics of the fiber-spinning process, along with subsequent efforts to develop theoretical models for specific spinning methods – such as ES, MS, and mechanical fiber drawing – plays a crucial role in predicting the scalability of the techniques and the quality of the materials produced. Most research has focused on ES configurations, leading to a substantial number of scientific papers that discuss the theoretical aspects of spinning in an electrostatic field.[151–153] In contrast, newer drawing techniques (MS, STEP, ThS, GD, *etc*.) have been only partially explored regarding the mechanics of fiber formation. Consequently, these investigations cannot be considered comprehensive. Some works,[116,139,141] among others, attempt to describe the dynamics of these processes.

To assess the scalability of a particular technique, it is essential to have experimental data supported by theoretical models. This helps in understanding several key factors: potential energy consumption and safety protocols resulting from external fields/forces applied, the construction costs of spinning devices, the rates of material production, and the compatibility of the technique with AM technologies that are used to fabricate multi-layer structures. The exemplary model for evaluating potential production rates using the force balance is Ziabicki's model,[148,149] which was developed for the experimental setup allowing for several types of spinning. In the experiment, the authors compared fiber-drawing velocities and material flow intensities between regular wet spinning and gravitational spinning. They found that the fiber-drawing (take-up) velocities for polycapronamide melts were 656 m min^{-1} and 210 m min^{-1}, respectively, both based on equal spinning paths of 450 cm. This indicates a slightly greater effectiveness of regular wet spinning compared with gravitational spinning. It is important to note that Ziabicki's model was the first to utilize and analyze the possibilities of gravitational spinning, preceding the first paper on gravity fiber drawing that was published in 2020.[147] In the next subsection of this review, we will primarily focus on the experimental data presented in recent studies to evaluate the scalability of various methods. This is necessary because the existing theoretical models remain incomplete for most of the recent drawing techniques.

The theoretical aspects of fiber-drawing processes help manage fiber serviceability, primarily represented by tunable fiber diameter, interfiber spacing, alignment, and structural and mechanical properties. The interfiber spacing (distance) is mainly controlled by precise systems of the spinning apparatus, such as motorized platforms for spinnerets and collectors. In contrast, fiber diameter and alignment are determined by the stability of the polymer stream as it travels along the spinning path. Hence, these parameters can be estimated using the force balance equation, which carefully considers the contributions from the rheological F_r, inertial F_i, surface F_s, and aerodynamical F_a constituents, along with several simplifications. The structural features of the filament formed during quenching are influenced by the stability of the stream and the length of the quench zone. While the degree of fiber crystallinity evaluated through differential scanning calorimetry (DSC) and/or X-ray diffraction (XRD) techniques is commonly considered the primary structural characteristic, a thorough investigation of the filament structure and the correlation between fiber crystallinity and mechanical properties remains to be explored. The subsection 3.3 Fiber serviceability will focus on assessing fiber serviceability through fiber fabrication techniques and the latest experimental data from published research.

3.2. Scalability of fiber fabrication techniques

In this review, we provide a clear analysis of the scalability of fiber-drawing techniques. We evaluate fiber production rates, consider the complexity of instrument configuration and associated production costs, and assess how compatible these techniques are with AM technologies. To build up the structure of the scalability analysis, we reference a study[141] which touches upon various ES and non-ES methods typically used in laboratory and industrial research.

3.2.1. Production rates. Fiber production rates can vary drastically based on the instrument configuration. Conventional single-needle homemade setups, mainly designed for lab-scale applications, typically employ solution or melt feed rates of 1–4 mL h^{-1}. These setups are not optimized for high output of materials for large-scale production. Therefore, the production rates for single-needle ES techniques usually fall between 0.01 to 0.3 g per h per nozzle.[154,155] Additionally, the rates for single-needle non-ES techniques have either not been accurately estimated or are reported to be below 0.2 g h^{-1}.[141,142] The introduction of gas-assisted and multi-nozzle systems can enhance production rates. For instance, one study[154] mentions an increase in fiber yield of up to 3.6 g h^{-1} when employing a gas-assisted spinneret configuration for the coaxial needle. Multi-jet systems can be adapted for various fiber-drawing techniques, significantly increasing fiber output. These systems are actively employed in methods such as ES, CS, ThS, and BS. By utilizing a combination of sheath gas and multiple nozzles, Zheng

et al.[76] reported a fiber output of 0.618–0.712 g h^{-1}, which is ~30–50 times higher than that of several conventional ES setups. Additionally, Tokarev *et al.*[139] successfully investigated multi-spinneret (multi-jet) systems for mechanical fiber drawing in both ThS and BS processes. A breakthrough in fiber-spinning techniques began with the introduction of advanced spinneret configurations, including rotating rollers that generate hundreds of jets in the electric field. This innovation led to the widespread adoption of needleless spinning methods – such as corona ES[156,157] and the aforementioned 'Nanospider' technology – which enable the formation of multiple jets across the electrode surface, thereby achieving exceptionally high fiber production yields. Thus, the 'Nanospider' technology allows for a fiber output of 90 g per h per unit length of the spinneret (electrode).[155] Considering the multi-electrode configuration – such as that offered by ELMARCO, s. r.o., where devices may incorporate up to 32 meter-long electrodes – the production rates can be readily scaled to kilogram-per-hour levels. Along with 'Nanospider' technology, Forcespinning, which utilizes CS principles, has been scaled up to achieve high fiber production rates of 60 g per h per unit length of the electrode.[141] Due to the process parameters, melt ES and, potentially, the recently introduced MMS can achieve higher production rates compared with solution ES techniques, reaching outputs of more than 75.6 g h^{-1}.[158]

The existing literature does not provide accurate information regarding the production rates for unconventional methods that employ magnetic, mechanical, and gravitational drawing principles. Consequently, the weight of material produced per unit of time remains poorly documented. However, for specific techniques like BS and GD, the authors have reported data on the fiber lengths that can be achieved. For instance, Tokarev *et al.*[139] documented a total length of 1700 km for PCL fibers produced during a five-minute BS process at 3000 rpm. Additionally, Yadavalli *et al.* highlighted the potential to fabricate meter-long PCL fibers using GD.[147] In a study[116] focused on MS, the authors measured the quantity of material produced by counting the number of fibers fabricated per unit of time at a specific rotation rate.

The experimental data on the STEP, ThS, BS, and GD methods demonstrate that the setups introduced – primarily designed for lab-scale research – do not match the productivity levels of commercial technologies like 'Nanospider'[159,160] and Forcespinning.[161,162] However, researchers at CytoNest, Inc. are currently exploring ways to enhance production by using larger devices equipped with multi-spinneret systems and bigger collection frames.[147,163] This exploration reveals the potential for achieving higher production rates with relatively inexpensive setups for mechanical and gravitational fiber drawing, even in the absence of external fields. As the GD method depends on gravitational force, it is characterized by lower production rates and is therefore considered inferior to mechanical drawing.

3.2.2. Instrument configuration and production costs. Most homemade setups for ES, magnetic field-assisted spinning, mechanical drawing, and gravitational drawing offer a cost-effective solution for proof-of-concept experiments. Typically, these setups can be built in a laboratory using 3D-printed components or inexpensive parts sourced from various vendors. The total cost of constructing the portable spinning apparatus in the laboratory ranges from a few hundred to a couple of thousand dollars, and maintenance expenses are generally low.[145,147,163,164] Although homemade fiber fabrication techniques offer various capabilities, their main drawback is the lack of reproducibility and batch-to-batch consistency, which arises from inadequate environmental control, insufficient coherence of apparatus components, and user safety concerns. Commercial devices are designed to achieve high consistency and reproducibility in fiber fabrication while ensuring user safety and providing excellent maintenance services. According to data from Inovenso, Vivolta, and FibeRio corporations, the price of large-scale production devices varies widely, ranging from about $10 000 to $250 000, depending on the instrument's configuration and capabilities. High-level ES and CS devices may cost more than $1 000 000. Currently, data on the commercialization efforts for mechanical and gravitational fiber-drawing techniques, including STEP, ThS, BS, and GD, are insufficient; therefore, equipment costs cannot be discussed in this review.

An important factor to consider when evaluating potential fiber production costs is the configuration of the power supply linked to the use of external fields or motorized systems, such as stepper motors or high-speed rotation nozzles/substrates. This consideration has become increasingly significant when replacing widely used ES techniques that rely on high-voltage power supply systems. A standard range for applied voltage in the ES is between 10 and 50 kV, with higher values for melt ES techniques.[158,165,166] The invention of NFES partially addressed the issue by reducing the applied voltage to 0.2–3 kV.[82] However, this method lacks high productivity and presents drawbacks, such as hindered fiber solidification and the formation of fibers with larger diameters resulting from short tip-to-collector distances. This prompted an investigation into the capabilities of mechanical fiber drawing, which began with CS. The CS devices, involving advanced Forcespinning technology, help lower production costs by functioning at low voltages ranging from 0.5 to 3 V.[167] However, the overall complexity of the instrument design (rotary machines developing high rotational speeds of up to 75 000 rpm) contributes to the high costs of the equipment itself. The development of STEP, ThS, and BS techniques can help address the challenges associated with complex apparatus design. Although these methods may have lower fiber productivity compared with the CS method, they have the potential for scalability. As reported, these techniques employ the principles of rotational and translational motion of substrates and spinnerets, which can be implemented using standard programmable controllers and DC motors operating at 6–24 V.[132] In summary, STEP, ThS, and BS techniques, which enable the production of aligned fiber patterns, appear to be strong candidates for scaling up. These methods have relatively low fiber production costs and benefit from simple instrument designs and principles that

can be applied to various polymer materials. Gravitational drawing, similar to unconventional mechanical drawing techniques, presents opportunities for creating precise fiber patterns, making it an appealing technology for scaling up. However, in contrast to mechanical drawing devices, GD setups contain complex systems for cutting and collecting fibers. These intricate systems, combined with lower production rates, pose challenges for integrating this method into large-scale production.[147]

The recently introduced technologies that utilize magnetic fields in fiber drawing are garnering less interest due to the added complexities involved in setting up instruments and preparing materials for spinning. Such spinning systems often require the integration of magnets or other sources to generate external magnetic fields. Furthermore, the spinning solutions or melts necessitate the addition of magnetic nanoparticles required to facilitate fiber stretching.[108,115,116] The synthesis of the nanoparticles is an extra and labor-intensive step in the material preparation process. On the other hand, purchasing pre-made inorganic nanoparticles adds to the overall costs. Considering the reported instrument designs and estimated low production rates, magnetic field-assisted methods are generally less appealing techniques compared with ES and mechanical drawing.

3.2.3. Compatibility with AM technologies. Tissue engineering strategies necessitate the creation of 3D NFS that mimic the architecture of the native ECM present in targeted tissues. To develop such a multi-layer structure, fiber arrays can be deposited layer by layer onto collecting substrates through multiple spinning cycles, as demonstrated in the STEP technique for producing small scaffolds.[136] Alternatively, individual fiber arrays can be stacked together using AM technologies (Fig. 15).

In AM approaches aimed at creating 3D structures, the first step usually involves extracting individual fiber layers from the collecting substrates after the spinning process.[147,163] Many common ES and CS technologies often struggle to tackle this challenge. ES techniques can use a variety of collecting substrates, including conductive, non-conductive, and combinations of both.[168,169] Conductive substrates, such as the commonly utilized aluminum foil, offer advantages over non-conductive collectors, as non-conductive collectors tend to accumulate charges over time, causing the fibers to disperse and generating lower packing densities. Regardless of the collector type, the technology requires mechanical fiber post-processing (extraction), which inevitably leads to fiber geometry distortions and fractures. The CS techniques developed to replace ES face similar challenges in the fiber extraction process. These challenges can be addressed for all four groups of methods, although with less success for ES, by adhering to the principles of direct fiber deposition on the intended substrates that will be stacked or further processed in scaffold manufacturing. The substrates are usually composed of non-toxic, biocompatible polymer materials with good mechanical properties, such as PLA and acrylonitrile butadiene styrene (ABS), and are created using digital modeling and 3D printing techniques.[140,147,163] The principles of direct writing onto intended substrates have been effectively applied in NFES,[170] SJES,[89] Melt ES,[166] and MMS.[117] However, utilizing these principles in ES presents difficulty in selecting the optimal substrate material.

3D printing technologies are essential for recent advancements in mechanical and gravitational fiber-drawing techniques. Research on methods such as STEP, ThS, BS, and GD highlights the importance of accurately designed static and dynamic collecting substrates (frames), spacers for fiber stacking, and other components of the instruments. These methods involve the direct deposition of aligned fiber arrays onto 3D-printed substrates with specified geometries, removing the fiber-extraction step that often leads to distortion in single-layer structures. Afterward, the substrates can be cut into smaller fragments using precise heating elements and 3D-printed spacers, which are typically made of the same material as the manufactured fibers. The spacers secure the edges of fiber arrays, preventing distortion and breakage. Later, these spacers with fibers are stacked layer by layer using heat presses, with temperatures adjusted to the melting point of the spacer material. This is one of the potential approaches outlined in the ThS and GD methods.[147,163]

It is important to admit that accurately modeling spacers with advanced software is crucial for developing a multi-layer structure. The geometry and thickness of the spacers significantly affect the overall efficiency of the scaffold and its ease of

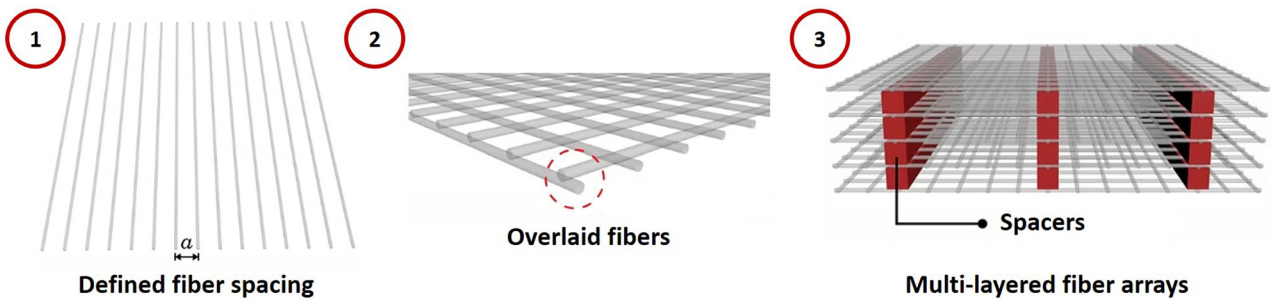

Fig. 15 Simple scheme for assembling aligned fiber arrays into an efficient multi-layered structure using AM technologies: 1 – fabrication of aligned fiber arrays using a particular drawing method, 2 – orthogonal alignment of two fiber arrays, 3 – construction of the multi-layered fiber structure utilizing spacers that can be melt together by heat press machine. The scheme has been provided by CytoNest, Inc.

use in the cell culture process. For instance, the size and shape of the spacers must be tailored to fit the specific dimensions of the cell culture dish or well. In lab-scale biological research, it is common to utilize 6-well plates and 12-well plates, each with its well size.[140,147,163] Therefore, the size of both spacer and scaffold must not exceed the dimensions of the wells. Additionally, the specific thickness of the spacer, which can range from tens of micrometers to several millimeters, defines the interlayer spacing. This spacing directly influences cell growth between layers in 3D NFS and the nutrient supply within them.

In this review, we argue that AM technologies are particularly significant for modern mechanical and gravitational drawing methods. Therefore, we conclude that these fiber fabrication methods exhibit the highest compatibility with AM compared with others.

3.3. Fiber serviceability

When developing an efficient 3D scaffold for cell culture, it is crucial to understand how a particular fiber-drawing technique influences the functionality of the resulting nano- and microfibers. Since the composition and organization of the ECM are specific to different tissues, the structural and biomechanical properties of the scaffolds produced may vary significantly. In ref. 177, Tonti *et al.* discuss tissue-specific characteristics of the ECM by examining examples from skin, nervous, kidney, skeletal muscle, and other tissues. Therefore, investigating how effectively the method can be adapted to produce fibers with tissue-specific properties is an integral part of analyzing the above techniques.

Current fiber and scaffold manufacturing techniques cannot accurately replicate the 3D structure of the native ECM with its tissue-specific fiber diameters, interfiber and interlayer spacing, and overall fiber organization within individual layers. However, with the help of AM, it becomes possible to create patterned polymer constructs that have defined fiber diameter, interfiber spacing, alignment, and other structural features, all of which influence the mechanical properties of the final material. For cell types that contribute to synthesizing and depositing ECM, such as fibroblasts, chondrocytes, osteoblasts, endothelial cells, *etc*., these precise constructs can serve as effective platforms for directing cell differentiation. In this subsection, we summarize the capabilities of the techniques applied to create aligned fiber patterns with adjustable fiber diameters and interfiber spacing. We also touch upon recent studies on the structure and mechanical properties of fibers produced using these methods.

3.3.1. Fiber diameter. Fiber diameter is a critical factor that affects fiber serviceability in tissue engineering applications. The thickness of individual fibers determines the active surface area available for cell attachment, as well as the mechanical properties of the fibers, such as tensile strength and elasticity modulus. Therefore, fiber-drawing techniques should enable precise control over fiber diameter at both the nanoscale and microscale, as required by the hierarchical architecture of the ECM. It is fair to say that most fiber fabrication methods provide ways to control fiber diameter through various solution (polymer concentration, flow rate, solvent evaporation rate) and process parameters (tip-to-collector distance, field intensity, rotational rate). We assume that all four groups of methods discussed within the framework of this review are capable of fabricating fibers with tunable diameters down to the nanometer scale. Thus, one study[178] presents an engineering approach for producing electrospun sub-nanometer fibers with adjustable diameters ranging from 0.17 to 0.63 nm using different concentrations of poly(acrylic acid). The BS technique[139] utilizing mechanical drawing principles successfully achieves tunable fiber diameters between 40 nm and 5 μm by adjusting the rotational speed and polymer concentration. Additionally, the recently introduced GD technique explores the potential for creating fibers with controlled diameters as small as ~400 nm.[147] These research works, among others discussed, demonstrate that various drawing techniques can achieve precise deposition of fibers with desired thickness.

The exceptions to the above-mentioned assumption are melt spinning techniques (Melt ES, MMS) and the NFES technique, which are known for producing thicker fibers. However, recent studies indicate that it is now possible to overcome the process limitations of these methods and produce nanofibers with tunable diameters.[99]

3.3.2. Interfiber spacing and alignment. Another key factor to consider when evaluating material serviceability is the aligned deposition of fibers with controlled interfiber spacing – frequently called 'porosity'. The interfiber spacing creates pathways for cell infiltration and ECM development. Controlled interfiber spacing within 3D structures plays a critical role in regulating nutrient supply, making it particularly important for studies involving the development of cell perfusion systems[179,180] that enable culture medium exchange within bioreactors. Such microfluidic systems are gaining significant attention, especially in the context of 3D NFS research, as they offer the potential to optimize the mesh size for improved tissue growth. Moreover, specific cell lines can produce and deposit ECM onto the surrounding environment. Therefore, the ideal network structure should encourage cell differentiation by promoting ECM production both on the fibers and in the spaces between them.

The data on commonly used cell lines in tissue engineering research (3T3/NIH fibroblasts, macrophages, human embryonic kidney cells, human umbilical vein endothelial cells, *etc*.) indicate that the average cell size typically ranges from 10 to 20 μm.[181–184] On one hand, small interfiber distances – less than or equal to the size of a single cell – are generally not optimal, as they immediately lead to cell overpopulation with subsequent formation of necrotic cores due to restricted nutrient diffusion. On the other hand, excessive interfiber spacing (greater than 100 μm) can hinder effective cell differentiation. While the optimal fibrous architecture may vary depending on the specific cell line, it is reasonable to suggest that, in most cases, a favorable interfiber spacing falls within the range of 10 to 50 μm. Therefore, the fiber fabrication method should

ensure a distribution of interfiber spacing that accommodates this range.

Fiber alignment, in turn, serves as a supporting parameter for tunable interfiber spacing. Most tissue-specific ECMs do not adhere to a precise geometric arrangement of fibers, and as a result, do not require a high level of alignment. However, certain cell cultures, such as neurons and smooth muscle cells, are highly sensitive to fiber alignment and tend to elongate and proliferate in a specific direction. This sensitivity paves the way for a focused area of research aimed at developing 3D scaffolds for culturing these direction-sensitive cell lines.

The majority of ES and CS methods currently used in the industry do not enable controlled deposition of aligned fiber patterns with specified interfiber spacing and instead produce randomly aligned fiber mats. Additionally, among the ES and magnetic field-assisted techniques, only the methods based on direct writing concepts (SJES, NFES, Melt ES, and MMS) allow for a high degree of alignment with adjustable interfiber spacing. These methods, however, have significant drawbacks, including larger fiber diameters (NFES, Melt ES, and MMS), limited applicability to biopolymers (Melt ES, MMS), and an overall complicated instrument configuration (Melt ES, MMS). The analysis of fiber fabrication techniques reveals that notable advancements in managing the spacing and alignment of fibers can be achieved through mechanical drawing methods, specifically STEP and ThS. These techniques result in a high degree of fiber alignment and consistent interfiber spacing due to the translational motion of spinnerets and/or collecting substrates. This precise translational motion is enabled by programmable stepper motors. Thus, a study on STEP-spun fibers[136] presents a technology for creating scaffolds with controlled porosity ranging from $80 \times 80\ \mu m^2$ to $5 \times 5\ \mu m^2$. In ref. 139, the authors explore the capabilities of ThS to produce square meshes with sizes as small as $5.8 \pm 1\ \mu m$. The assembly of fiber arrays with a tunable interfiber spacing of 20–1000 μm has been demonstrated in gravitational fiber drawing,[147] as it utilizes collector motion principles similar to those in mechanical drawing.

3.3.3. Considerations on structural and mechanical properties. The research on fiber structure and its relationship to mechanical properties remains a complex issue in materials science that has not been sufficiently covered in the existing literature. In published studies, the authors often highlight the crystallinity degree as the primary characteristic when discussing the structure of fibers produced using a specific spinning technique. The degree of fiber crystallinity is typically determined through DSC and XRD experiments, providing some insight into the material's structure. This critical parameter has been studied across various polymer materials, and recent works on electrospun fibers for biomedical research indicate that the crystallinity degree usually does not exceed 65%.[185–187] However, a significant issue arises from the predominant focus on electrospun fibers, creating a gap in research regarding the structure of fibers obtained through other methods. Currently, only a few studies have attempted to conduct a comparative analysis of fiber crystallinity based on materials fabricated using different drawing techniques. For example, one study[186] compared the degree of crystallinity in fibers manufactured through needle-based ES, needleless ES, solution CS, and melt CS. Additionally, Lee *et al.*[140] explored the structural characteristics of touch-spun and electrospun PCL fibers and found that mechanically drawn fibers exhibited higher crystallinity and elastic modulus.

Since the degree of crystallinity contributes to material density, elastic modulus, and other mechanical properties at the microscale, this parameter is assumed to play a key role in biomechanical processes involving material–cell interactions.

The mechanical properties of 3D scaffolds are primarily influenced by the characteristics of the fibers used. Generally, the upper limits for the elastic modulus and tensile strength of these fibers are about 10 GPa and 1 GPa, respectively.[188] These values either match or even surpass the mechanical properties of natural collagen fibers found in the ECM. It is important to highlight that the mechanical characteristics of nanofibers produced by unconventional drawing techniques have not yet been reported, which limits our understanding of the biomechanical principles involved in cell culture. Furthermore, examining the mechanics of individual nanofilaments poses significant challenges that can be partially addressed through the precise technique of atomic force microscopy indentation.

4. Conclusions and future perspectives

Growing interest in developing scaffolds for 3D cell cultures has been stimulated by the need to develop 3D tissues and efficient cell manufacturing technologies. To meet this demand, new fiber-spinning techniques such as STEP and ThS have emerged, offering both scalability and control over fiber characteristics, including fiber alignment within well-assembled 3D architectures. These methods have exhibited cost-effective and scalable approaches to create fiber arrays with precise diameters, interfiber spacing, and mechanical properties. The significance of research focused on developing optimal materials for efficient, long-term cell culture and subsequent tissue formation extends beyond tissue engineering, with potential applications in the emerging field of cellular agriculture. Modern cellular agriculture approaches involve the production of lab-grown meat and seafood and rely on similar cell culture techniques. In this context, advances in the development of well-assembled 3D nano- and microfiber scaffolds are clearly beneficial for both fields, offering a shared technological foundation for regenerative medicine and sustainable food production.

One of the major questions that may arise in the context of designing 3D scaffolds for tissue engineering is: why is it necessary to tune fiber alignment? When addressing this concern, it is important to acknowledge that the role played by fiber alignment in tissue-specific ECM remains an active and

evolving area of biomedical research. While certain tissues lack well-defined fiber organization, others critically depend on aligned fiber architectures, which have been shown to influence cell behavior through biomechanical mechanisms that are not yet fully illustrated. This has been demonstrated, for example, in neuronal and smooth muscle cells. The central premise is that, if 3D scaffolds can be engineered to fulfill all key structural criteria – optimal fiber diameter, interfiber spacing, and alignment – this would facilitate broader investigation of nano- and microfiber materials, even for tissue types where alignment is not a primary requirement. From a strategic perspective, we propose that research should begin by tackling the most demanding structural scenarios. This, in turn, raises two major challenges in tissue development: first, a limited understanding of the signaling mechanisms that govern direction-sensitive cell growth; and second, the need to investigate the mechanical properties of individual nano- or microfilaments. The latter has been partially addressed using techniques such as wide-angle X-ray diffraction, atomic force microscopy (AFM) nanoindentation, and complex AFM–optical microscopy systems.

The advancements in fiber fabrication techniques hold significant promise for tissue engineering, and are expected to be integrated with AM methods to enable rapid production of 3D scaffolds. Achieving this integration will require the development of efficient spinning and scaffolding systems capable of continuous operation. This includes strategies such as using individual nano- and microfiber sheets as structural building blocks (as seen in GD and ThS) or depositing fibers directly during the drawing process. A key ongoing challenge lies in the automation of nanofiber drawing and handling, especially for achieving precise control over fiber properties and positioning during scaffold assembly. Therefore, we envision more collaboration between mechanical engineers, polymer scientists, and cell biologists to develop platforms that can automate fiber drawing and assembly into biologically relevant architectures. This approach will ultimately accelerate the translation of engineered scaffolds into functional tissue constructs.

Scalable methods for fabricating well-defined 3D scaffolds have only recently become available. However, our understanding of how cells respond to these scaffolds, how manufacturing parameters influence scaffold properties, and how these factors can be effectively integrated into cell culture applications remains limited. In particular, the interplay between the viscoelastic properties of individual fibers, their spatial organization within 3D architectures, and the resulting effects on cellular behavior has not yet been systematically explored or engineered.

Author contributions

Kristina Peranidze: conceptualization, project administration, writing – original draft, writing – review & editing. Nataraja Yadavalli: writing – original draft. Brianna Blevins: writing – original draft. Mikhail Parker: writing – original draft. Tushita Jain: writing – original draft. Mohammad Aghajohari: writing – original draft, writing – review & editing. Sergiy Minko: funding acquisition, project administration, supervision, writing – review & editing. Vladimir Reukov: funding acquisition, project administration, supervision, writing – review & editing.

All authors have given approval to the final version of the manuscript.

Conflicts of interest

The authors declare no competing financial interest.

Data availability

No primary research results, software or code have been included and no new data were generated or analyzed as part of this review.

Acknowledgements

This work has been partially supported by the funds from the Georgia Research Alliance grant no. RGRA1000174300A. M. A. was supported by the U.S. Department of Energy, Office of Science, Office of Biological and Environmental Research program under award no. DE-SC0023338. N.S.Y. acknowledges the awards of the USDA National Institute of Food and Agriculture STTR Program, USA (grant no. 2023-51402-39329) and the Good Food Institute for the support of 3D scaffold development.

References

1 W. Cui, Y. Zhou and J. Chang, Electrospun nanofibrous materials for tissue engineering and drug delivery, *Sci. Technol. Adv. Mater.*, 2010, **11**(1), 014108.
2 R. CeCe, *et al.*, An Overview of the Electrospinning of Polymeric Nanofibers for Biomedical Applications Related to Drug Delivery, *Adv. Eng. Mater.*, 2024, **26**(1), 2301297.
3 P. Phutane, *et al.*, Biofunctionalization and applications of polymeric nanofibers in tissue engineering and regenerative medicine, *Polymers*, 2023, **15**(5), 1202.
4 B. Qiu, *et al.*, 3D Aligned Nanofiber Scaffold Fabrication with Trench-Guided Electrospinning for Cardiac Tissue Engineering, *Langmuir*, 2024, **40**(9), 4709–4718.
5 D. A. Sánchez-Téllez, *et al.*, Novel PVA–Hyaluronan–Siloxane Hybrid Nanofiber Mats for Bone Tissue Engineering, *Polymers*, 2024, **16**(4), 497.
6 E. Diep and J. D. Schiffman, Living Antimicrobial Wound Dressings: Using Probiotic-Loaded, Alginate Nanofibers for Protection against Methicillin-Resistant Staphylococcus aureus, *ACS Appl. Bio Mater.*, 2024, **7**(2), 787–790.
7 X. Zhang, *et al.*, Advances in wound dressing based on electrospinning nanofibers, *J. Appl. Polym. Sci.*, 2024, **141**(1), e54746.

8 A. Y. Darwesh, *et al.*, Advanced 3D Electrospinning "Xspin" System: Fabrication of Bifiber Floating Oral Pharmaceutical Scaffolds for Controlled Drug Delivery, *Mol. Pharm.*, 2024, **21**(2), 916–931.
9 H. Samadian, *et al.*, Multi-effect formulation based on pH-Responsive psyllium Mucilage/Poly (vinyl alcohol) nanofibers for controlled delivery of mesalamine, *J. Drug Delivery Sci. Technol.*, 2024, **92**, 105348.
10 X. Li, *et al.*, Fabricating polyacrylonitrile-polyethyleneimine nanofiber membranes with exceptional hemocompatibility and efficient bilirubin removal for hemoperfusion, *React. Funct. Polym.*, 2024, **194**, 105793.
11 D. Yu, *et al.*, Recent Advances in Stimuli–Responsive Smart Membranes for Nanofiltration, *Adv. Funct. Mater.*, 2023, **33**(9), 2211983.
12 X. Dong, *et al.*, Aligned Nanofibers Promote Myoblast Polarization and Myogenesis through Activating Rac-Related Signaling Pathways, *ACS Biomater. Sci. Eng.*, 2024, **10**(3), 1712–1721.
13 T. Ebbinghaus, G. Lang and T. Scheibel, Biomimetic polymer fibers—function by design, *Bioinspiration Biomimetics*, 2023, **18**(4), 041003.
14 A. Randhawa, *et al.*, Manufacturing 3D Biomimetic Tissue: A Strategy Involving the Integration of Electrospun Nanofibers with a 3D–Printed Framework for Enhanced Tissue Regeneration, *Small*, 2024, 2309269.
15 C. S. Baldwin, S. Iyer and R. R. Rao, The challenges and prospects of smooth muscle tissue engineering, *Regen. Med.*, 2024, **19**(3), 135–143.
16 T. J. Hawke and F. Zaucke, *Exploring frontiers in musculoskeletal biology and bioengineering*, American Physiological Society, Rockville, MD, 2024.
17 X. Lin, *et al.*, The bone extracellular matrix in bone formation and regeneration, *Front. Pharmacol.*, 2020, **11**, 521497.
18 J. Eschweiler, *et al.*, The biomechanics of cartilage—An overview, *Life*, 2021, **11**(4), 302.
19 L. E. Eisner, *et al.*, The role of the non-collagenous extracellular matrix in tendon and ligament mechanical behavior: a review, *J. Biomech. Eng.*, 2022, **144**(5), 050801.
20 N. L. Leong, *et al.*, Tendon and ligament healing and current approaches to tendon and ligament regeneration, *J. Orthop. Res.*, 2020, **38**(1), 7–12.
21 R. Velu, *et al.*, A Comprehensive Review on Bio-Nanomaterials for Medical Implants and Feasibility Studies on Fabrication of Such Implants by Additive Manufacturing Technique, *Materials*, 2020, **13**(1), 92.
22 N. N. Potekaev, *et al.*, The role of extracellular matrix in skin wound healing, *J. Clin. Med.*, 2021, **10**(24), 5947.
23 J. Labat-Robert, A.-M. Robert and L. Robert, Aging of the extracellular matrix, *Medec. Longev.*, 2012, **4**(1), 3–32.
24 M. Rabbani, N. Zakian and N. Alimoradi, Contribution of physical methods in decellularization of animal tissues, *J. Med. Signals Sens.*, 2021, **11**(1), 1–11.
25 P. Xu, *et al.*, Recent advances in fabrication of dECM-based composite materials for skin tissue engineering, *Front. Bioeng. Biotechnol.*, 2024, **12**, 1348856.
26 A. Coyle, *et al.*, Developing Bioactive Hydrogels Containing Cell-derived Extracellular Matrix: Implications in Drug and Cell-free Bone and Cartilage Repair, *bioRxiv*, 2024, preprint, DOI: **10.1101/2024.03.04.583366**.
27 B.-S. Kim, *et al.*, Comparative analysis of supercritical fluid-based and chemical-based decellularization techniques for nerve tissue regeneration, *Biomater. Sci.*, 2024, **12**, 1847–1863.
28 Y. Shu, *et al.*, Three-dimensional printing and decellularized-extracellular-matrix based methods for advances in Artificial Blood Vessel fabrication: A Review, *Tissue Cell*, 2024, 102304.
29 Q. Mao, *et al.*, Fabrication of liver microtissue with liver decellularized extracellular matrix (dECM) bioink by digital light processing (DLP) bioprinting, *Mater. Sci. Eng., C*, 2020, **109**, 110625.
30 J. W. Kim, *et al.*, Kidney decellularized extracellular matrix enhanced the vascularization and maturation of human kidney organoids, *Adv. Sci.*, 2022, **9**(15), 2103526.
31 O. Janoušková, Synthetic polymer scaffolds for soft tissue engineering, *Physiol. Res.*, 2018, **67**(2), 335–348.
32 M. J. Javid-Naderi, *et al.*, Synthetic polymers as bone engineering scaffold, *Polym. Adv. Technol.*, 2023, **34**(7), 2083–2096.
33 L. Suamte, A. Tirkey and P. J. Babu, Design of 3D smart scaffolds using natural, synthetic and hybrid derived polymers for skin regenerative applications, *Smart Mater. Med.*, 2023, **4**, 243–256.
34 A. Barhoum, *et al.*, Nanofibers as new-generation materials: From spinning and nano-spinning fabrication techniques to emerging applications, *Appl. Mater. Today*, 2019, **17**, 1–35.
35 N. Mohan and M. S. Detamore, Biomimetic nanofibers for musculoskeletal tissue engineering, in *Nanotechnology Applications for Tissue Engineering*, Elsevier, 2015, pp. 57–75.
36 J. K. Kular, S. Basu and R. I. Sharma, The extracellular matrix: Structure, composition, age-related differences, tools for analysis and applications for tissue engineering, *J. Tissue Eng.*, 2014, **5**, 2041731414557112.
37 P. Cai, *et al.*, Elastic 3D-Printed Nanofibers Composite Scaffold for Bone Tissue Engineering, *ACS Appl. Mater. Interfaces*, 2023, **15**(47), 54280–54293.
38 O. A. González Rodríguez, *et al.*, Polycaprolactone, polylactic acid, and nanohydroxyapatite scaffolds obtained by electrospinning and 3D printing for tissue engineering, *Int. J. Polym. Mater. Polym. Biomater.*, 2023, 1–12.
39 D. Kharaghani, *et al.*, The effect of polymeric nanofibers used for 3D-printed scaffolds on cellular activity in tissue engineering: a review, *Int. J. Mol. Sci.*, 2023, **24**(11), 9464.
40 F. Bafande and M. Sheikh Arabi, Features and methods of making nanofibers by electrospinning, phase separation and self-assembly, *Jorjani Biomed. J.*, 2022, **10**(1), 13–25.
41 J. Zhao, *et al.*, Preparation and properties of biomimetic porous nanofibrous poly (l-lactide) scaffold with chitosan nanofiber network by a dual thermally induced phase sep-

aration technique, *Mater. Sci. Eng., C*, 2012, **32**(6), 1496–1502.
42 E. Stojanovska, *et al.*, A review on non-electro nanofibre spinning techniques, *RSC Adv.*, 2016, **6**(87), 83783–83801.
43 M. Zahmatkeshan, *et al.*, *Polymer-based nanofibers: preparation, fabrication, and applications*, in *Handbook of nanofibers*, Springer, 2019, pp. 215–261.
44 L. Fan, *et al.*, Facile In Situ Assembly of Nanofibers within Three-Dimensional Porous Matrices with Arbitrary Characteristics for Creating Biomimetic Architectures, *Nano Lett.*, 2023, **23**(18), 8602–8609.
45 G. Pandey, *et al.*, Supramolecular self-assembled peptide-engineered nanofibers: A propitious proposition for cancer therapy, *Int. J. Biol. Macromol.*, 2023, 128452.
46 A. N. Dickson, K.-A. Ross and D. P. Dowling, Additive manufacturing of woven carbon fibre polymer composites, *Compos. Struct.*, 2018, **206**, 637–643.
47 D. K. Rajak, *et al.*, Fiber-reinforced polymer composites: Manufacturing, properties, and applications, *Polymers*, 2019, **11**(10), 1667.
48 J. Xue, *et al.*, Electrospinning and electrospun nanofibers: Methods, materials, and applications, *Chem. Rev.*, 2019, **119**(8), 5298–5415.
49 I. Topolniak, *et al.*, High–Precision Micropatterning of Polydopamine by Multiphoton Lithography, *Adv. Mater.*, 2022, **34**(18), 2109509.
50 C. Liu, Z. Xia and J. T. Czernuszka, Design and development of three-dimensional scaffolds for tissue engineering, *Chem. Eng. Res. Des.*, 2007, **85**(7), 1051–1064.
51 D. J. Mech and M. S. Rizvi, Micromechanics of fibrous scaffolds and their stiffness sensing by cells, *Biomed. Mater.*, 2024, **19**(2), 025035.
52 M. Abbasipour and R. Khajavi, Nanofiber bundles and yarns production by electrospinning: a review, *Adv. Polym. Technol.*, 2013, **32**(3), 21363.
53 N. Sultana, *et al.*, *Scaffold fabrication protocols*, in *Composite synthetic scaffolds for tissue engineering and regenerative medicine*, 2015, pp. 13–24.
54 G. K. Sharma and N. R. James, Progress in electrospun polymer composite fibers for microwave absorption and electromagnetic interference shielding, *ACS Appl. Electron. Mater.*, 2021, **3**(11), 4657–4680.
55 D. H. Reneker and A. L. Yarin, Electrospinning jets and polymer nanofibers, *Polymer*, 2008, **49**(10), 2387–2425.
56 A. Hiwrale, *et al.*, Nanofibers: A current era in drug delivery system, *Heliyon*, 2023, **9**(9), 18917.
57 K. Peranidze, T. V. Safronova and N. R. Kildeeva, Fibrous polymer-based composites obtained by electrospinning for bone tissue engineering, *Polymers*, 2021, **14**(1), 96.
58 H. Niu, X. Wang and T. Lin, Upward needleless electrospinning of nanofibers, *J. Eng. Fibers Fabr.*, 2012, **7**(2_suppl), 155892501200702S03.
59 J. I. Kim, *et al.*, A controlled design of aligned and random nanofibers for 3D bi-functionalized nerve conduits fabricated via a novel electrospinning set-up, *Sci. Rep.*, 2016, **6**(1), 23761.
60 J. A. Matthews, *et al.*, Electrospinning of collagen nanofibers, *Biomacromolecules*, 2002, **3**(2), 232–238.
61 H. Pan, *et al.*, Continuous aligned polymer fibers produced by a modified electrospinning method, *Polymer*, 2006, **47**(14), 4901–4904.
62 T. Lei, *et al.*, New insight into gap electrospinning: toward meter-long aligned nanofibers, *Langmuir*, 2018, **34**(45), 13788–13793.
63 N. Rivoallan, *et al.*, Graded electrospun scaffold from aligned fibers to honeycomb micropatterns: Application to bone-tendon tissue engineering, *Biomater. Adv.*, 2025, 214413.
64 Y. Liu, *et al.*, *Scale-up strategies for electrospun nanofiber production*, in *Electrospun and Nanofibrous Membranes*, Elsevier, 2023, pp. 205–266.
65 Y. Wang, *et al.*, Tri-layer core–shell fibers from coaxial electrospinning for a modified release of metronidazole, *Pharmaceutics*, 2023, **15**(11), 2561.
66 S. Anjum, *et al.*, Bioinspired core-shell nanofiber drug-delivery system modulates osteogenic and osteoclast activity for bone tissue regeneration, *Mater. Today Bio*, 2024, **26**, 101088.
67 S. Shafizadeh, *et al.*, Coaxial electrospun PGS/PCL and PGS/PGS-PCL nanofibrous membrane containing platelet-rich plasma for skin tissue engineering, *J. Biomater. Sci., Polym. Ed.*, 2024, **35**(4), 482–500.
68 R. A. Macartney, *et al.*, Co-delivery of VEGF and amoxicillin using LP-coated co-axial electrospun fibres for the potential treatment of diabetic wounds, *Biomater. Adv.*, 2024, **158**, 213765.
69 W. He, *et al.*, Integrating coaxial electrospinning and 3D printing technologies for the development of biphasic porous scaffolds enabling spatiotemporal control in tumor ablation and osteochondral regeneration, *Bioact. Mater.*, 2024, **34**, 338–353.
70 I. G. Kim, *et al.*, A comprehensive electric field analysis of cylinder-type multi-nozzle electrospinning system for mass production of nanofibers, *J. Ind. Eng. Chem.*, 2015, **31**, 251–256.
71 W. Tomaszewski and M. Szadkowski, Investigation of electrospinning with the use of a multi-jet electrospinning head, *Fibre Text. East. Eur.*, 2005, **13**(4), 22.
72 Y. Yang, *et al.*, A shield ring enhanced equilateral hexagon distributed multi-needle electrospinning spinneret, *IEEE Trans. Dielectr. Electr. Insul.*, 2010, **17**(5), 1592–1601.
73 A. Valipouri, Production scale up of nanofibers: a review, *J. Text. Polym.*, 2017, **5**(1), 8–16.
74 M. Fan, *et al.*, Electric field simulation of multi-needle water bath electrospinning and the structural properties of SCN/PAN micro/nanofiber composite yarns, *Nanotechnology*, 2023, **34**(50), 505702.
75 B. E. Kwak, *et al.*, Large-scale centrifugal multispinning production of polymer micro-and nanofibers for mask filter application with a potential of cospinning mixed multicomponent fibers, *ACS Macro Lett.*, 2021, **10**(3), 382–388.

76 G. Zheng, *et al.*, Multinozzle high efficiency electrospinning with the constraint of sheath gas, *J. Appl. Polym. Sci.*, 2019, **136**(22), 47574.
77 H. S. SalehHudin, *et al.*, Simulation and experimental study of parameters in multiple-nozzle electrospinning: Effects of nozzle arrangement on jet paths and fiber formation, *J. Manuf. Process.*, 2021, **62**, 440–449.
78 N. Joy, *et al.*, Coupling between voltage and tip-to-collector distance in polymer electrospinning: Insights from analysis of regimes, transitions and cone/jet features, *Chem. Eng. Sci.*, 2021, **230**, 116200.
79 K. D. Patel, *et al.*, Basic concepts and fundamental insights into electrospinning, in *Biomedical Applications of Electrospinning and Electrospraying*, Elsevier, 2021, pp. 3–43.
80 X.-X. He, *et al.*, Near-field electrospinning: progress and applications, *J. Phys. Chem. C*, 2017, **121**(16), 8663–8678.
81 G. Zheng, *et al.*, Precision deposition of a nanofibre by near-field electrospinning, *J. Phys. D: Appl. Phys.*, 2010, **43**(41), 415501.
82 G. S. Bisht, *et al.*, Controlled continuous patterning of polymeric nanofibers on three-dimensional substrates using low-voltage near-field electrospinning, *Nano Lett.*, 2011, **11**(4), 1831–1837.
83 D. Li, *et al.*, Preparation and Characterization of Novel Multifunctional Wound Dressing by Near-Field Direct-Writing Electrospinning and Its Application, *Polymers*, 2024, **16**(11), 1573.
84 H. Yuan, *et al.*, Stable jet electrospinning for easy fabrication of aligned ultrafine fibers, *J. Mater. Chem.*, 2012, **22**(37), 19634–19638.
85 Y. Zhang, *et al.*, Chitosan nanofibers from an easily electrospinnable UHMWPEO-doped chitosan solution system, *Biomacromolecules*, 2008, **9**(1), 136–141.
86 H. A. Christ, *et al.*, Production of highly aligned microfiber bundles from polymethyl methacrylate via stable jet electrospinning for organic solid–state lasers, *J. Polym. Sci.*, 2022, **60**(4), 715–725.
87 Z. Guo and Z. Wu, Well-aligned Polycaprolactone Fiber by Stable Jet Electrospinning, *J. Phys.: Conf. Ser.*, 2021, **1906**(1), 012036.
88 S. Lei, *et al.*, Stable-jet length controlling electrospun fiber radius: Model and experiment, *Polymer*, 2019, **180**, 121762.
89 B. Yi, *et al.*, Fabrication of high performance silk fibroin fibers via stable jet electrospinning for potential use in anisotropic tissue regeneration, *J. Mater. Chem. B*, 2018, **6**(23), 3934–3945.
90 Q. Zhou, *et al.*, Implication of stable jet length in electrospinning for collecting well-aligned ultrafine PLLA fibers, *Polymer*, 2013, **54**(25), 6867–6876.
91 H. Yuan, *et al.*, Direct printing of patterned three-dimensional ultrafine fibrous scaffolds by stable jet electrospinning for cellular ingrowth, *Biofabrication*, 2015, **7**(4), 045004.
92 P. Babinec and O. Jirsak, Microwave absorbing nonwoven textile from electrospun magnetically responsive nanofibres, *Optoelectron. Adv. Mater., Rapid Commun.*, 2008, **2**, 474–477.
93 F. Yalcinkaya, B. Yalcinkaya and O. Jirsak, Dependent and independent parameters of needleless electrospinning, in *Electrospinning–Material, Techniques and Biomedical Applications*, 2016, pp. 67–93.
94 F. Yener and O. Jirsak, Improving performance of polyvinyl butyral electrospinning, in *Proceedings of the 4th International Nanocon Conference*, 2011.
95 A. Karpińska, A. Simaite and M. Buzgo, Theoretical Models of the Most Promising Needle-Free Electrospinning Systems for Drug Delivery Applications, *Proceedings*, 2021, **78**(1), 33.
96 K. K. Peranidze, *et al.*, Biocompatible composite films and fibers based on Poly (Vinyl alcohol) and powders of calcium salts, *Smart Mater. Med.*, 2021, **2**, 292–301.
97 C. Mouro, A. P. Gomes and I. C. Gouveia, Emulsion electrospinning of PLLA/PVA/chitosan with Hypericum perforatum L. as an antibacterial Nanofibrous wound dressing, *Gels*, 2023, **9**(5), 353.
98 T. D. Brown, P. D. Dalton and D. W. Hutmacher, Melt electrospinning today: An opportune time for an emerging polymer process, *Prog. Polym. Sci.*, 2016, **56**, 116–166.
99 C. Mingjun, *et al.*, An example of industrialization of melt electrospinning: Polymer melt differential electrospinning, *Adv. Ind. Eng. Polym. Res.*, 2019, **2**(3), 110–115.
100 S. B. Qasim, *et al.*, Electrospinning of chitosan-based solutions for tissue engineering and regenerative medicine, *Int. J. Mol. Sci.*, 2018, **19**(2), 407.
101 M. A. Obeid, *et al.*, Formulation of polycaprolactone meshes by melt electrospinning for controlled release of daunorubicin in tumour therapy, *Colloids Surf., A*, 2024, **699**, 134873.
102 C. Böhm, *et al.*, Processing of Poly (lactic–co–glycolic acid) Microfibers via Melt Electrowriting, *Macromol. Chem. Phys.*, 2022, **223**(5), 2100417.
103 Y. Wang, *et al.*, Green and highly efficient preparation of superfine fiber yarns via vortex airflow-assisted melt differential electrospinning, *Composites, Part A*, 2025, **189**, 108552.
104 L. Larrondo and R. St. John Manley, Electrostatic fiber spinning from polymer melts. I. Experimental observations on fiber formation and properties, *J. Polym. Sci., Polym. Phys. Ed.*, 1981, **19**(6), 909–920.
105 A. Karchin, *et al.*, Melt electrospinning of biodegradable polyurethane scaffolds, *Acta Biomater.*, 2011, **7**(9), 3277–3284.
106 T. Blachowicz and A. Ehrmann, Most recent developments in electrospun magnetic nanofibers: A review, *J. Eng. Fibers Fabr.*, 2020, **15**, 1558925019900843.
107 F. Kashani-Asadi-Jafari, A. Parhizgar and A. Hadjizadeh, Magnetic-field-assisted emulsion electrospinning system: designing, assembly, and testing for the production of pcl/gelatin core–shell nanofibers, *Fibers Polym.*, 2023, **24**(2), 515–523.
108 Y. Liu, *et al.*, Magnetic field-assisted electrospinning of aligned straight and wavy polymeric nanofibers, *Adv. Mater.*, 2010, **22**(22), 2454.

109 A. F. Khusnuriyalova, *et al.*, Preparation of cobalt nanoparticles, *Eur. J. Inorg. Chem.*, 2021, **2021**(30), 3023–3047.
110 C. Stavilă, *et al.*, Enhancement of chemotherapy effects by non-lethal magneto-mechanical actuation of gold-coated magnetic nanoparticles, *Nanomedicine*, 2024, 102766.
111 J. Kurimský, *et al.*, Electric partial discharges in biodegradable oil-based ferrofluids: A study on effects of magnetic field and nanoparticle concentration, *Heliyon*, 2024, **10**(7), 29259.
112 J. Philip, Magnetic nanofluids (Ferrofluids): Recent advances, applications, challenges, and future directions, *Adv. Colloid Interface Sci.*, 2023, **311**, 102810.
113 A. Joseph and S. Mathew, Ferrofluids: synthetic strategies, stabilization, physicochemical features, characterization, and applications, *ChemPlusChem*, 2014, **79**(10), 1382–1420.
114 S. Lysenko, *et al.*, Structural organization of magnetic fluids stabilized with fatty acids, *Inorg. Mater.: Appl. Res.*, 2018, **9**, 334–342.
115 A. Tokarev, *et al.*, Reactive Magnetospinning of Nano–and Microfibers, *Angew. Chem.*, 2015, **127**(46), 13817–13820.
116 A. Tokarev, *et al.*, Magnetospinning of nano–and microfibers, *Adv. Mater.*, 2015, **27**(23), 3560–3565.
117 K. Zhang, *et al.*, A new magnetic melt spinning device for patterned nanofiber, *Sci. Rep.*, 2021, **11**(1), 8895.
118 H. Lee, *et al.*, Handspinning enabled highly concentrated carbon nanotubes with controlled orientation in nanofibers, *Sci. Rep.*, 2016, **6**(1), 37590.
119 D. Jao and V. Z. Beachley, Continuous dual-track fabrication of polymer micro-/nanofibers based on direct drawing, *ACS Macro Lett.*, 2019, **8**(5), 588–595.
120 K. Sarkar, *et al.*, Electrospinning to forcespinning™, *Mater. Today*, 2010, **13**(11), 12–14.
121 H. Xu, *et al.*, A review on current nanofiber technologies: Electrospinning, centrifugal spinning, and electro–centrifugal spinning, *Macromol. Mater. Eng.*, 2023, **308**(3), 2200502.
122 J. Ahmed, M. Gultekinoglu and M. Edirisinghe, Recent developments in the use of centrifugal spinning and pressurized gyration for biomedical applications, *Wiley Interdiscip. Rev.: Nanomed. Nanobiotechnol.*, 2024, **16**(1), e1916.
123 A. M. Loordhuswamy, *et al.*, Fabrication of highly aligned fibrous scaffolds for tissue regeneration by centrifugal spinning technology, *Mater. Sci. Eng., C*, 2014, **42**, 799–807.
124 H. Zhou, *et al.*, Cotton-like micro-and nanoscale poly (lactic acid) nonwoven fibers fabricated by centrifugal melt-spinning for tissue engineering, *RSC Adv.*, 2018, **8**(10), 5166–5179.
125 F. L. Dantas, *et al.*, PLLA Scaffolds Functionalized with Ketoprofen via Rotary Jet Spinning for Biomedical Applications, *J. Mater. Res. Technol.*, 2024, **30**, 9020–9027.
126 D. Miele, *et al.*, Design and development of polydioxanone scaffolds for skin tissue engineering manufactured via green process, *Int. J. Pharm.*, 2023, **634**, 122669.
127 L. Vera, *et al.*, Osteoinductive 3D scaffolds prepared by blend centrifugal spinning for long-term delivery of osteogenic supplements, *RSC Adv.*, 2018, **8**(39), 21889–21904.
128 S. Feng, *et al.*, Preparation and characterization of SA/AKP composite fibers by centrifugal wet continuous spinning, *Mater. Today Commun.*, 2023, **35**, 105514.
129 I. Alghoraibi and S. Alomari, Different methods for nanofiber design and fabrication, in *Handbook of nanofibers*, 2018, vol. 1, p. 46.
130 S. M. H. Marjuban, *et al.*, Recent advances in centrifugal spinning and their applications in tissue engineering, *Polymers*, 2023, **15**(5), 1253.
131 R. Huang, *et al.*, Facile one-step synthesis of PVDF bead-on-string fibers by pressurized gyration for reusable face masks, *Polymers*, 2022, **14**(21), 4498.
132 A. S. Nain, *et al.*, Dry spinning based spinneret based tunable engineered parameters (STEP) technique for controlled and aligned deposition of polymeric nanofibers, *Macromol. Rapid Commun.*, 2009, **30**(16), 1406–1412.
133 A. S. Nain, *et al.*, Control of cell behavior by aligned micro/nanofibrous biomaterial scaffolds fabricated by spinneret–based tunable engineered parameters (STEP) technique, *Small*, 2008, **4**(8), 1153–1159.
134 A. S. Nain, *et al.*, Drawing suspended polymer micro-/nanofibers using glass micropipettes, *Appl. Phys. Lett.*, 2006, **89**(18), 183105.
135 K. Sheets, *et al.*, Cell-fiber interactions on aligned and suspended nanofiber scaffolds, *J. Biomater. Tissue Eng.*, 2013, **3**(4), 355–368.
136 J. Wang and A. S. Nain, Suspended micro/nanofiber hierarchical biological scaffolds fabricated using non-electrospinning STEP technique, *Langmuir*, 2014, **30**(45), 13641–13649.
137 Z. Gu, *et al.*, Fiber diameters and parallel patterns: proliferation and osteogenesis of stem cells, *Regen. Biomater.*, 2023, **10**, rbad001.
138 A. C. Dotivala, K. P. Puthuveetil and C. Tang, Shear force fiber spinning: process parameter and polymer solution property considerations, *Polymers*, 2019, **11**(2), 294.
139 A. Tokarev, *et al.*, Touch-and brush-spinning of nanofibers, *Adv. Mater.*, 2015, **27**(41), 6526–6532.
140 S.-J. Lee, *et al.*, Touch-spun nanofibers for nerve regeneration, *ACS Appl. Mater. Interfaces*, 2019, **12**(2), 2067–2075.
141 L. F. Deravi, *et al.*, Design and fabrication of fibrous nanomaterials using pull spinning, *Macromol. Mater. Eng.*, 2017, **302**(3), 1600404.
142 J. Uribe-Gomez, *et al.*, Soft elastic fibrous scaffolds for muscle tissue engineering by touch spinning, *ACS Appl. Bio Mater.*, 2021, **4**(7), 5585–5597.
143 M. F. Ismail, *et al.*, High–Throughput Production of Gelatin–Based Touch–Spun Nanofiber for Biomedical Applications, *Adv. Eng. Mater.*, 2024, **26**(23), 2401022.
144 W. Kitana, *et al.*, Biofabrication of Composite Bioink–Nanofiber Constructs: Effect of Rheological Properties of Bioinks on 3D (Bio) Printing and Cells Interaction with

Aligned Touch Spun Nanofibers, *Adv. Healthcare Mater.*, 2024, **13**(6), 2303343.

145 J. K. Sandridge, *et al.*, Fabricating Synthetic, Small-diameter Vascular Templates via Touch-spinning, *J. Mech. Behav. Biomed. Mater.*, 2025, 107010.

146 J. Uribe-Gomez, *et al.*, Fibrous Scaffolds for Muscle Tissue Engineering Based on Touch–Spun Poly (Ester–Urethane) Elastomer, *Macromol. Biosci.*, 2022, **22**(4), 2100427.

147 N. S. Yadavalli, *et al.*, Gravity Drawing of Micro–and Nanofibers for Additive Manufacturing of Well–Organized 3D–Nanostructured Scaffolds, *Small*, 2020, **16**(11), 1907422.

148 A. Ziabicki and K. Kedzierska, Mechanical aspects of fibre spinning process in molten polymers: Part I. stream diameter and velocity distribution along the spinning way, *Kolloid-Z.*, 1960, **171**, 51–61.

149 A. Ziabicki and K. Kedzierska, Mechanical aspects of fibre spinning process in molten polymers: Part II. Stream broadening after the exit from the channel of spinneret, *Kolloid-Z.*, 1960, **171**, 111–119.

150 Z. K. Walczak, *Processes of fiber formation*, Elsevier, 2002.

151 Y. Guo, *et al.*, Research progress, models and simulation of electrospinning technology: A review, *J. Mater. Sci.*, 2022, 1–47.

152 S. Rafiei, *et al.*, Mathematical modeling in electrospinning process of nanofibers: a detailed review, *Cellul. Chem. Technol.*, 2013, **47**(5), 323–338.

153 C. Ru, *et al.*, A novel mathematical model for controllable near-field electrospinning, *AIP Adv.*, 2014, **4**(1), 017108.

154 D. Han and A. J. Steckl, Coaxial electrospinning formation of complex polymer fibers and their applications, *ChemPlusChem*, 2019, **84**(10), 1453–1497.

155 S. Omer, *et al.*, Scale-up of electrospinning: Market overview of products and devices for pharmaceutical and biomedical purposes, *Pharmaceutics*, 2021, **13**(2), 286.

156 B. Farkas, *et al.*, Corona alternating current electrospinning: A combined approach for increasing the productivity of electrospinning, *Int. J. Pharm.*, 2019, **561**, 219–227.

157 M. Kaneko, *et al.*, Charging properties of atactic poly (styrene) microfibre mats charged with electrospinning and corona charging, *Smart Mater. Struct.*, 2024, **33**(9), 095043.

158 M. Chen, *et al.*, Polymer melt differential electrospinning from a linear slot spinneret, *J. Appl. Polym. Sci.*, 2020, **137**(31), 48922.

159 B. A. Dages, *et al.*, Edible electrospun materials for scalable cultivated beef production, *Food Bioprod. Process.*, 2025, **149**, 118–129.

160 Y. Ma, *et al.*, Research progress and industrial application of electrostatic spinning nanofibers in foods, *Food Eng. Rev.*, 2025, **17**(1), 1–26.

161 T. Khan, S. Raza and S. Bala, Exploration of Advances in Sustainable Nanomaterials in Textile Industries, in *Sustainable Nanomaterials: Synthesis and Environmental Applications*, Springer, 2024, pp. 339–356.

162 J. Reinoza, *et al.*, Fabrication of pullulan-chitosan fiber membranes for enhanced hemostatic applications, *Int. J. Biol. Macromol.*, 2025, **308**, 142552.

163 M. M. Uddin, *et al.*, Fabrication of Aligned Polyhydroxybutyrate Fibrous Scaffolds via a Touchspinning Apparatus, *ACS Omega*, 2025, **10**(11), 22735–22746.

164 J. Lv, *et al.*, Controllable fabrication of high-quality magnetic nanofiber membranes using variable magnetic field-assisted electrospinning technology, *Polymer*, 2025, **321**, 128130.

165 K. Koenig, F. Langensiepen and G. Seide, Pilot-scale production of polylactic acid nanofibers by melt electrospinning, *e-Polymers*, 2020, **20**(1), 233–241.

166 Q. Xia, *et al.*, Study on the Melt Electrospinning Method with Internal Electrode and Fiber Refinement, *Fibers Polym.*, 2025, 1–10.

167 L. Alvarado-Ramírez, *et al.*, Synthesis of polymeric fibers incorporated with pineapple peel with potential antioxidant and anti-inflammatory application in the cosmetic industry, *Reactions*, 2024, **7**, 8.

168 C. Hellert, *et al.*, Positioning and aligning electrospun PAN fibers by conductive and dielectric substrate patterns, in *Macromolecular Symposia*, Wiley Online Library, 2021.

169 H. Nishiuchi and H. Tonami, Control of mat thickness in electrospinning with transparent conductive glass collector, *Polym. Eng. Sci.*, 2022, **62**(7), 2252–2259.

170 F. Mohtaram, *et al.*, Near-Field Direct Write Electrospinning of PET-Carbon Quantum Dot Solutions, *Materials*, 2024, **17**(24), 6242.

171 A.-L. Gürtler, *et al.*, Coaxial electrospinning of polycaprolactone–A design of experiments approach, *Eur. Polym. J.*, 2024, **208**, 112886.

172 Y.-K. Wu, *et al.*, Multi-jet electrospinning with auxiliary electrode: The influence of solution properties, *Polymers*, 2018, **10**(6), 572.

173 G. Zheng, *et al.*, Nanofiber membranes by multi-jet electrospinning arranged as arc-array with sheath gas for electrodialysis applications, *Mater. Des.*, 2020, **189**, 108504.

174 W. E. King III and G. L. Bowlin, Near-field electrospinning and melt electrowriting of biomedical polymers—Progress and limitations, *Polymers*, 2021, **13**(7), 1097.

175 Y. Zhang, *et al.*, Stable multi-jet electrospinning with high throughput using the bead structure nozzle, *RSC Adv.*, 2018, **8**(11), 6069–6074.

176 Q. Hao, *et al.*, Gravity-Driven Ultrahigh-Speed Electrospinning for the Production of Ethyl Cellulose Fibers with Tunable Porosity for Oil Absorption, *ACS Sustainable Chem. Eng.*, 2024, **13**(1), 507–517.

177 O. R. Tonti, *et al.*, Tissue-specific parameters for the design of ECM-mimetic biomaterials, *Acta Biomater.*, 2021, **132**, 83–102.

178 S. Jian, *et al.*, Nanofibers with diameter below one nanometer from electrospinning, *RSC Adv.*, 2018, **8**(9), 4794–4802.

179 H. Kimura, *et al.*, Standalone cell culture microfluidic device-based microphysiological system for automated

cell observation and application in nephrotoxicity tests, *Lab Chip*, 2024, **24**(3), 408–421.

180 G. Wu, *et al.*, A novel microfluidic self-perfusion chip (MSPC) for pumpless 3D cell, microtissue and organoid culture, *Lab Chip*, 2025, **25**, 3694–3706.

181 A. Amirsadeghi, *et al.*, Melt Electrowriting of Elastic Scaffolds Using PEOT–PBT Multi–block Copolymer, *Adv. Healthcare Mater.*, 2025, **14**(3), 2402914.

182 M. Liu, *et al.*, Preparation and Characterization of Crimped PLA Fibers With Surface Porous Structure to Promote Cell Adhesion and Growth, *J. Appl. Polym. Sci.*, 2025, **142**(7), e56540.

183 Y. Matsumura, *et al.*, Incorporation of Adeno-Associated Virus Encoding Vascular Endothelial Growth Factor into a Biodegradable Elastomeric Scaffold for Improved Function in the Ischemic Rat Heart, *ACS Biomater. Sci. Eng.*, 2025, **11**(4), 2226–2235.

184 Y. Wang, *et al.*, Electrospun Silk Fibroin–Silk Sericin Scaffolds Induced Macrophage Polarization and Vascularization for Volumetric Muscle Loss Injury, *J. Funct. Biomater.*, 2025, **16**(2), 56.

185 O. Ero-Phillips, M. Jenkins and A. Stamboulis, Tailoring crystallinity of electrospun plla fibres by control of electrospinning parameters, *Polymers*, 2012, **4**(3), 1331–1348.

186 E. Kuzelova Kostakova, *et al.*, Crystallinity of electrospun and centrifugal spun polycaprolactone fibers: a comparative study, *J. Nanomater.*, 2017, **2017**(1), 8952390.

187 N. Q. Nguyen, T.-F. Chen and C.-T. Lo, Confined crystallization and chain conformational change in electrospun poly (ethylene oxide) nanofibers, *Polym. J.*, 2021, **53**(8), 895–905.

188 T. U. Rashid, R. E. Gorga and W. E. Krause, Mechanical properties of electrospun fibers—a critical review, *Adv. Eng. Mater.*, 2021, **23**(9), 2100153.